Allen Brain Observatory – Neuropixels Visual Coding

TECHNICAL WHITE PAPER: OVERVIEW

The Allen Brain Observatory comprises a set tools and protocols for carrying out comprehensive surveys of *in vivo* neural activity during sensory stimulation and behavior. The first round of Brain Observatory data collection used two-photon imaging to measure activity across a range of cell types in six cortical areas in response to a standardized battery of visual stimuli (de Vries et al., 2018). Now, the Brain Observatory has been extended to include experiments with Neuropixels, a device capable of recording spiking activity with high temporal resolution at any depth within the mouse brain. For the initial Neuropixels data release, responses have been measured from neurons across the visual cortex, hippocampus, and thalamus utilizing wild-type C57BL6/J mice and transgenic Cre lines expressing channelrhodopsin in inhibitory interneuron sub-types (Sst-IRES-Cre; Ai32, Pvalb-IRES-Cre; Ai32 and Vip-IRES-Cre; Ai32). This dataset will serve as a valuable resource for exploring the coding of sensory stimuli at both the single-cell and population levels, as well as studying neural interactions within and between the areas under investigation.

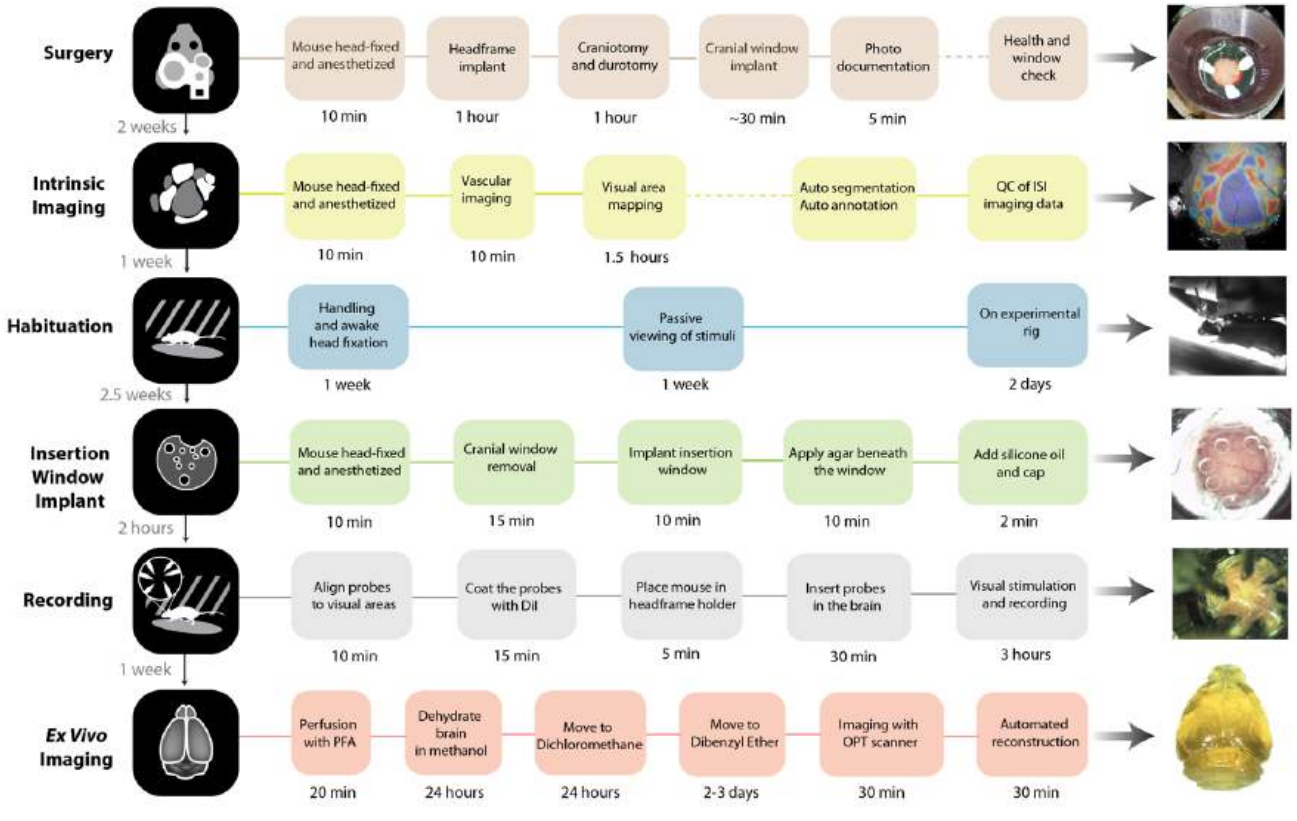

Figure 1. The Allen Brain Observatory Neuropixels workflow. The pipeline consists of six major steps: (1) a surgical procedure to implant a custom headframe and insert a glass window over visual cortex; (2) intrinsic signal imaging to identify cortical visual areas; (3) habituation of mice to head fixation and visual stimulation; (4) replacement of the glass window with a plastic window containing holes for inserting probes; (5) an *in vivo* extracellular electrophysiology experiment; and (6) recovery of recording locations using optical projection tomography (OPT). The details and approximate duration of each step are described in each row.

The data acquisition and processing pipeline utilized standardized operating procedures (SOPs), custom instrumentation, and workflows conducive to scaling. Functionally defined visual areas were targeted for study via intrinsic signal imaging (ISI) and neuronal activity was measured by *in vivo* extracellular electrophysiology (**Figure 1**) in response to a battery of visual stimuli. Data are available in standardized Neurodata Without Borders (NWB) format via the AllenSDK. The Allen Institute has served as a founding scientific partner in the effort to develop the NWB standard, a unified data format for neurophysiology data (Teeters et al., 2015).

This document provides an overview of data acquisition, data analysis, and quality control procedures used for this resource. All experimental work described in this paper was performed with approval and oversight of the Allen Institute Institutional Animal Care and Use Committee. The Allen Institute holds an Animal Welfare Assurance with the Public Health Service (PHS) and complies with all applicable aspects of the *PHS Policy on Humane Care of Laboratory Animals* and the *Guide for the Care and Use of Laboratory Animals*.

DATA ACQUISITION

MICE

Wild-type C57BL/6J mice were purchased from Jackson Laboratories at age P25-50. For experiments involving opto-tagging of inhibitory cells, Pvalb-IRES-Cre, Vip-IRES-Cre, and Sst-IRES-Cre mice were bred in-house and crossed to an Ai32 reporter line (Madisen et al., 2012). Pvalb-IRES-Cre; Ai32 breeding sets (pairs and trios) consisted of heterozygous Pvalb-IRES-Cre mice mated to either heterozygous or homozygous Ai32(RCL-ChR2(H134R)_EYFP) mice. Pvalb-IRES-Cre is expressed in the male germline. To avoid germline deletion of the stop codon in the LoxP-STOP-LoxP cassette, Pvalb-IRES-Cre; Ai32 mice were not used as breeders. Sst-IRES-Cre; Ai32 breeding sets (pairs and trios) consisted of heterozygous Sst-IRES-Cre mice mated to either heterozygous or homozygous Ai32(RCL-ChR2(H134R)_EYFP) mice. Vip-IRES-Cre; Ai32 breeding sets (pairs and trios) consisted of heterozygous Vip-IRES-Cre mice mated to either heterozygous or homozygous Ai32(RCL-ChR2(H134R)_EYFP) mice. Cre+ cells from Ai32 lines are highly photosensitive, due to expression of Channelrhodopsin-2 (Zhang et al., 2006).

SURGERY

Headframe Design

To enable data co-registration across multiple imaging and electrophysiology rigs, each animal was implanted with a stereotaxically aligned headframe that provides a cranial window for brain imaging and permits head fixation in a reproducible configuration. An integrated suite of tools (data acquisition rigs, mouse behavior platforms, and implant alignment hardware) was developed to enable the identical presentation of stimuli across different instruments, and to register data acquired from different instruments. All measurements are referenced to a plane passing through lambda and bregma and the mediolateral axis (origin at lambda). Initial measurements showed that the cranial window angle was at 23 degrees of roll, and 6 degrees of pitch. To achieve standardization, a head-frame implant (**Figure 2**) was designed to provide registration relative to lambda and to enable head-fixation at a controlled angle. Use of a custom fixture enabled placement of the headframe such that the craniotomy could be repeatability centered at x = –2.8 mm and y = 1.3 mm on the reference plane.

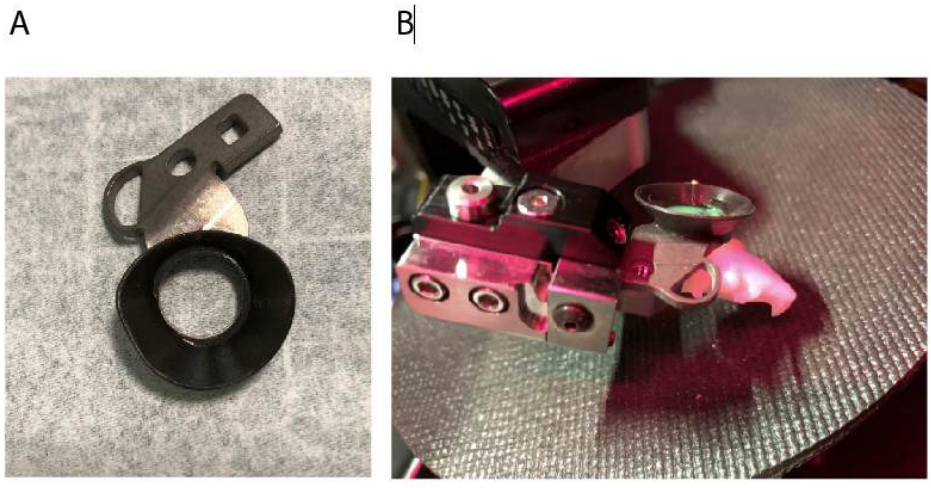

Figure 2. Headframe for cross-platform registration. (A) A 304 stainless steel headframe contains a 10 mm diameter opening for accessing the brain, while providing a durable reference surface for clamping. A printed well was made from a black acrylic photopolymer to shield the probes and provide a surface for mounting the plastic insertion window used during the experiment. Headframes were assembled in a jig to ensure uniform offset between the center of the well and the reference surfaces of the clamp and joined with Loctite 406. (**B**) Headframe clamp that allows the mouse's head to be reproducibly aligned across rigs. The headframe is mounted against the shaft of the shoulder-bolt (center) and the back face of the clamp by the flat-head screw (right) which acts as a wedge. The shoulder-bolt and tertiary clamp bolt (left) were tightened to finalize installation and constrain the clamp-plate against the large flat registration surface of the clamp. Instruments were calibrated using a headframe that contained a reticle at the nominal center position of the cranial window.

Cranial Window Surgery

Mice received a headframe and cranial coverslip implant 4-5 weeks prior to recording. Pre-operative injections of dexamethasone (3.2 mg/kg, S.C.) were administered at 12h and 3h before surgery. Mice were initially anesthetized with 5% isoflurane (1-3 min) and placed in a stereotaxic frame (Model# 1900, Kopf, Tujunga, CA), and isoflurane levels were maintained at 1.5-2.5% for surgery. An incision was made to remove skin, and the exposed skull was levelled with respect to pitch (bregma-lamda level), roll and yaw. The stereotaxic frame was calibrated to lambda using a custom headframe holder equipped with a stylus affixed to a clamp-plate. The stylus was then replaced with the headframe to center the headframe well at 3.1 mm lateral and 1.3 mm anterior to lambda. The headframe was affixed to the skull with white C&B Metabond (Parkell). Once the Metabond was dry, the mouse was placed in a custom clamp to position the skull at a rotated angle of 20º, to facilitate creation of the craniotomy over visual cortex. A circular piece of skull 5 mm in diameter was removed, and a durotomy was performed. The skull was replaced by a 5 mm thick circular glass coverslip (**Figure 3,** left). The bottom of the coverslip was coated with silicone to reduce adhesion to the brain surface. The cranial coverslip was secured to the skull with Vetbond (Goldey et al., 2014). Kwik-Cast (World Precision Instruments) was added around the coverslip to further seal the implant (**Figure 3**, right). Following surgery, mice entered a 7-10 recovery period that included regular checks for overall health, cranial window clarity, and brain health. Post-surgical brain health was documented using a custom photo-documentation system to acquire a spatially registered image of the cranial window.

Surgery Quality Control

Out of 105 mice entering surgery, 4 did not pass on to the next step in the pipeline. The main reasons for QC failure were procedure failures (the mouse did not survive the surgery) or poor brain health during the post-operative surgical checks.

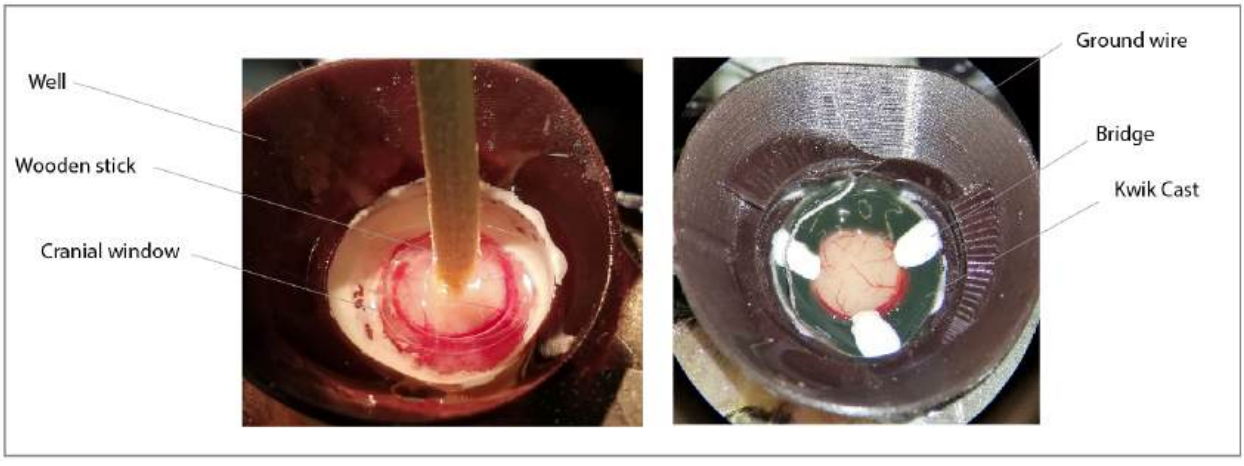

Figure 3. Cranial window surgery. Left, image of glass cranial window implantation. Right, the cranial window after sealing sealed with Vetbond and Kwik Cast. Metabond bridges (in white) make contact between the headframe well and the cranial window to add stability.

INTRINSIC SIGNAL IMAGING (ISI)

Intrinsic signal imaging (ISI) measures the hemodynamic response of the cortex to visual stimulation across the entire field of view. This technique can be used to obtain retinotopic maps representing the spatial relationship of the visual field (or in this case, coordinate position on the stimulus monitor) to locations within each cortical area. This mapping procedure was used to delineate functionally defined visual area boundaries to enable targeting of Neuropixels probes to retinotopically defined locations in primary and secondary visual areas (Juavinett et al., 2017).

ISI Data Acquisition

Animal preparation. Mice were lightly anesthetized with 1-1.4% isoflurane administered with a SomnoSuite (model #715; Kent Scientific, CON) at a flow rate of 100 ml/min supplemented with ~95% O_2 concentrated air (Pureline OC4000; Scivena Scientific, OR). Vital signs were monitored with a PhysioSuite (model # PS-MSTAT-RT; Kent Scientific). Eye drops (Lacri-Lube Lubricant Eye Ointment; Refresh) were applied to maintain hydration and clarity of the eye during anesthesia. Mice were placed on a lab jack platform and head-fixed for imaging normal to the cranial window. The headframe and clamping mechanism ensured consistent and accurate positioning of the mouse eye in relation to the stimulus screen from experiment to experiment.

Image Acquisition System. To map the retinotopic organization of the cortex and standardize data acquisition, an ISI system coupled to visual stimulation was assembled. The brain surface was illuminated with a ring of sequential and independent LED lights, with green (peak λ = 527nm; FWHM = 50nm; Cree Inc., C503B-GCN-CY0C0791) and red spectra (peak λ = 635nm and FWHM of 20 nm; Avago Technologies, HLMP-EG08-Y2000) mounted on the optical lens. A pair of Nikon lenses operated front-to-front with a back lens (Nikon Nikkor 105mm f/2.8), and a front lens (Nikon Nikkor 35mm f/1.4), provided 3.0x magnification (M = 105/35). The back focal plane of the 50 mm lens was adjacent and coplanar to the cranial window (working distance, 46.5 mm), and was equipped with a bandpass filter (Semrock; FF01-630/92 nm) to selectively allow longer wavelengths of reflected light to reach the camera sensor and to filter screen contamination and ambient light. Illumination and image time series acquisition were controlled with custom software written in Python. An Andor Zyla 5.5 10 tap sCMOS camera was used at a frame rate of 40 Hz with frame intervals timed using the camera's hardware clock running at 40 MHz. Initiation of simultaneous image acquisition and visual stimulus display was hardware-triggered from a National Instruments Digital IO board. Frames of 2560 x 2160 pixels and a 16-bit dynamic range were saved to disk at a 4x4 spatial binning and 4x temporal binning, resulting in 640x640 pixels/frame, 10Hz time series, 32-bit dynamic range and a resulting effective pixel size of 10 μm.

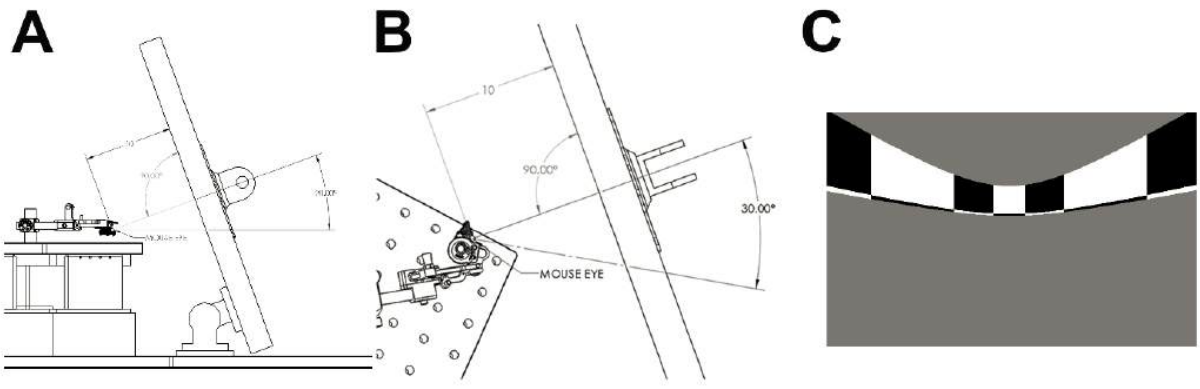

Figure 4. Visual stimulus screen placement and presentation. (A) Side view of the experimental setup showing the center of the monitor positioned at 10 cm away from the eye of the mouse. The monitor was also tilted 70° to the horizontal to present the stimulus parallel to the retina. **(B)** Aerial view of the position of the stimulus monitor showing the screen positioned 30° from the mouse dorsoventral axis also contributing to the parallel relationship between the retina and stimulus display. **(C)** Example snapshot of the stimulus presented, here showing a horizontal sweep moving downwards.

Visual Stimulus for ISI

The lambda-bregma axis of the skull, as positioned in the head frame clamp, was oriented with a 30° pitch relative to horizontal, corresponding to a horizontal eye position ~60° lateral to midline and a vertical position ~20° above the horizon (Oommen and Stahl, 2008). To ensure maximal coverage of the field of view, a 24" monitor was positioned 10 cm from the right eye. The monitor was rotated 30° relative to the animal's dorsoventral axis and tilted 70° off the horizon to ensure that the stimulus was perpendicular to the optic axis of the eye (**Figure 4A,B**). The visual stimulus was comprised of a drifting bar containing a checkerboard pattern, alternating black and white as it sweeps along a gray background (**Figure 4C**). The stimulus bar sweeps across the four cardinal axes 10 times in each direction at a rate of 0.1 Hz (Kalatsky and Stryker, 2003). The drifting bar measures 20° by 155°, with individual square sizes measuring at 25º. The stimulus was warped spatially so that a spherical representation could be displayed on a flat monitor (Marshel et al., 2011).

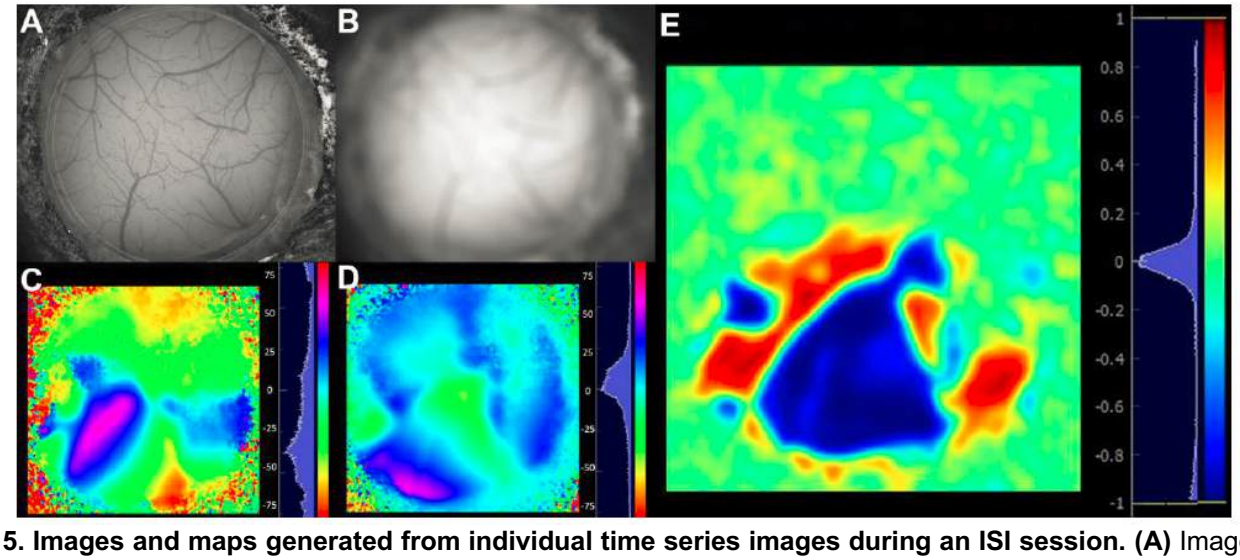

Figure 5. Images and maps generated from individual time series images during an ISI session. (A) Image of the vasculature in focus, used to register the ISI map with the Neuropixels insertion site. **(B)** Image at the slightly defosed plane used for ISI. **(C)** Azimuth map computed from horizontal sweeps of the drifting bar stimulus, with scale bar in degrees. **(D)** Altitude map computed from vertical sweeps of the drifting bar stimulus, with scale bar in degrees. **(E)** Visual sign map showing area boundaries, generated from the sine of the angle between the horizontal and vertical map gradients.

Image Acquisition & Processing

An in-focus image of the surface vasculature was acquired with green LED illumination to provide a fiduciary marker reference on the surface of the visual cortex. After defocusing from the surface vasculature (between 500 μm and 1500 μm along the optical axis), up to 10 independent ISI time series were acquired and used to measure the hemodynamic response to visual stimulus-induced brain activity. The resulting images were first processed to maximize the signal-to-noise ratio using time-averaged pixel direct current (DC) signal removal. A Discrete Fourier Transform (DFT) at the stimulus frequency was performed on the pre-processed images. Phase maps were generated by calculating the phase angle of the pre-processed DFT at the stimulus frequency and then used to translate the location of a visual stimulus from the retina to cortical spatial anatomy. A sign map was produced from the phase maps by taking the sine of the angle between the altitude and azimuth map gradients. **Figure 5** shows an example of the vasculature images and computed maps obtained for one mouse. Averaged sign maps were produced from a minimum of three time series images for a combined minimum average of 30 stimulus sweeps in each direction.

ISI Curation and Data Processing

Automated Sign Map Segmentation and Annotation. An automated segmentation and annotation module was developed to delineate boundaries between visual areas. For each experiment, a visual field sign map was computed as the sine of the angle between the horizontal and vertical map gradients. Negative values (visualized in blue in **Figure 5E**) represent a mirror image of the visual field while positive values (red) represent a non-mirror image. The sign map is automatically segmented into distinct visual areas with an algorithm (based on algorithm in (Garrett et al., 2014) that used three criteria to segregate visual areas: 1) each area must contain the same visual field sign; 2) each area cannot have a redundant representation of visual space; 3) adjacent areas of the same visual field sign must have a redundant representation. To facilitate automated annotation, a set of 35 ISI experiments were used to build an initial map of 12 major cortical visual areas (VISp, VISpl, VISl, VISli, VISal, VISlla, VISrl, VISam, VISpm, VISmma, VISmmp, VISm). The identity of each area was first manually annotated to provide “ground truth” identification (**Figure 6**). Each sign map was aligned to a canonical space by shifting the center of mass of the primary visual cortex, V1, to the origin, and rotating the image so that the direction of the altitude retinotopy gradient of primary visual area was horizontal and consistent across experiments. Statistics for area sign, location, size, and spatial relationships were compiled.

Subsequent ISI datasets were automatically segmented, and the automated annotation algorithm compared the sign, location, size, and spatial relationships of the segmented areas against those compiled in the ISI-derived atlas of visual areas. A cost function, defined by the discrepancy between the properties of the matched areas, was minimized to identify the best match between visual areas in the experimental sign map and those in the atlas, resulting in an auto-segmented and annotated map for each experiment. The automated ISI segmentation and annotation modules achieved ~97% accuracy on a pilot dataset. Manual correction and editing of the results included merging and splitting of segmented and annotated areas to correct errors.

Eccentricity and Target Map Generation. Two eccentricity maps were generated (**Figure 6 D,E**). The first is a map of eccentricity from the center of visual space, at the intersection of 0° altitude and 0° azimuth (**Figure 6D**). If the retina is centered on the origin of the visual stimulus at the center of the monitor, the center of visual space (in stimulus coordinates of altitude and azimuth) should fall approximately on the anatomical center of V1, corresponding to the center of the retina. For example, if the optic axis of the eye was pointed at the upper portion of the screen rather than the center of the stimulus (the origin, 0° altitude and azimuth in screen coordinates), the values of the altitude map would be shifted upwards, resulting in a corresponding shift in the origin of the map of visual eccentricity away from V1’s center. The value of retinotopic eccentricity at the V1 centroid was used as a QC criterion, as described below, to identify experiments where the eye significantly deviated from the center of the stimulus (>15º shift).

The maps of altitude and azimuth represent a mapping of the screen onto the retina. Accordingly, the exact values and range of the maps vary across experiments as a result of differences in eye position relative to the monitor. To provide a reliable map for subsequent targeting of Neuropixels probes, a consistent anatomical coordinate corresponding to the center of V1 (which maps to center of the retina) was used to realign the maps. A map of eccentricity from the V1 centroid was produced by shifting the origin of the map of visual eccentricity **(Figure 6D)** to the coordinates at the V1 centroid, showing the retinotopic gradients relative to this point (**Figure 6E**). A representation of the corresponding retinotopic location is present in nearly all higher visual areas (**Figure 6F**, indicated in red in the heat map). Using this location as the target for electrophysiology experiments ensures that recorded neurons represent a consistent region on the retina, approximately at the center of the right visual hemifield.

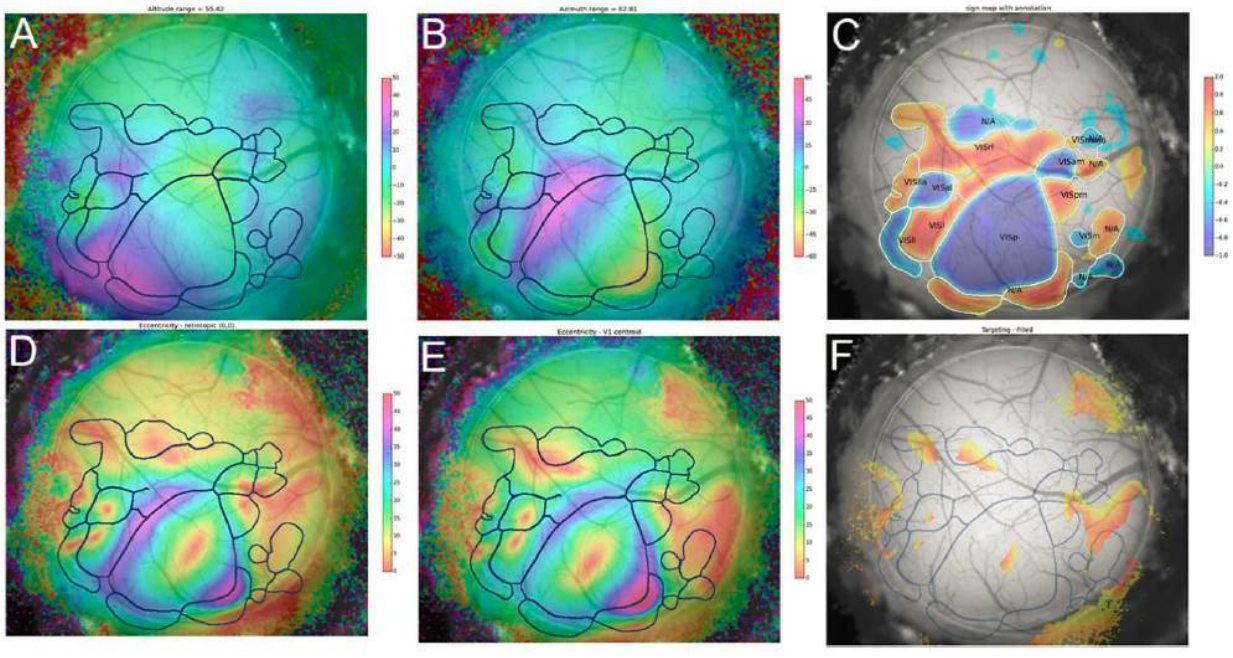

Figure 6. Images and averaged maps generated post-acquisition. All selected trials are averaged to produce azimuth **(A)** and altitude **(B)** maps, and a map of visual field sign with segmented area boundaries overlaid on a vasculature image **(C)**. From the altitude and azimuth maps and segmented area boundaries, a map of visual eccentricity **(D)**, a map of eccentricity from the V1 centroid **(E),** and a target map **(F)** are computed. List of acronyms: Primary Visual Area (VISp), Posterolateral visual area (VISpl), Laterointermediate area (VISli), Lateral visual area (VISl), Anteromedial visual area (VISal), Laterolateral anterior visual area (VISlla), Rostrolateral visual area (VISrl), Anteromedial visual area (VISam), Posteromedial visual area (VISpm), Medial visual area (VISm), Mediomedial anterior visual area (VISmma), Mediomedial posterior visual area (VISmmp). Scale bar in degrees for A, B, D & E.

To provide a discrete target location for Neuropixels probe insertion, targeting maps were created from the maps of eccentricity at the center of V1 **(Figure E)** by restricting the map to values of eccentricity that are within 10 degrees from the origin. In addition, the target map was limited to retinotopic values that are negative for both altitude and azimuth. This gives the target a specific directionality, displaying values only for the lower peripheral quadrant of visual space to bias the targeting closer to the center of the Neuropixels rig's visual display monitor. This targeting map **(Figure 6F)** was overlaid on an image of the surface vasculature to provide fiducial landmarks to facilitate co-registration with images of the brain surface taken during the experiment.

ISI Quality Control

The quality control process for the ISI-derived maps included four distinct inspection steps (**Figure 7**):

1. The brain surface and vasculature images were inspected post-acquisition for clarity, focus, and position of the cranial window within the field of view (QC-1).

2. Individual trials were inspected for visual coverage range and continuity of phase maps, localization of the signal from the amplitude maps and stereotypical organization of sign maps. Only trials respecting these criteria were included in the final average, and a minimum of 3 trials were required (QC-2).

3. Visual area boundaries were delineated using automated segmentation, and maps were curated based on stringent criteria to ensure data quality. The automated segmentation and identification of a minimum of six visual areas including VISp, VISlm, VISrl, VISal, VISam and VISpm was required (**see Figure 7**). A maximum of three manual adjustments were permitted to compensate for algorithm inefficiency (QC-3).

4. Each processed retinotopic map was inspected for coverage range (35-60° altitude and 60-100° azimuth), bias (absolute value of the difference between max and min of altitude or azimuth range; <10°), alignment of the center of retinotopic eccentricity with the centroid of V1 (<15° apart; **Fig. 7E, F**), and the area size of V1 (>2.8 cm_2).

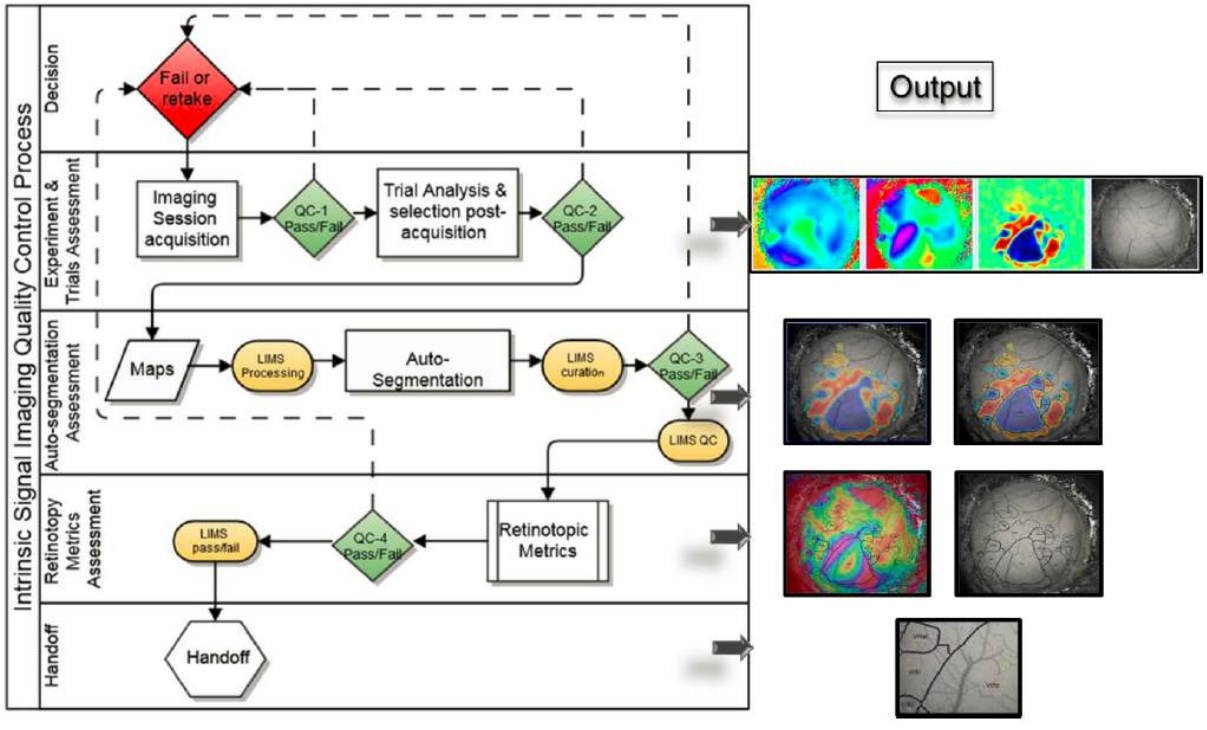

Figure 7. Schematic of ISI process and quality control. Beginning at "Imaging session acquisition", a number of process and QC steps were followed, each resulting in the maps shown to the right.

In addition to the QC procedures carried out on the ISI-derived maps, the vasculature images were also examined. The presence of white artifacts on the brain surface, an indicator of potential brain damage, was grounds for failing the mouse out of the pipeline.

Out of 101 mice entering ISI, 9 did not pass onto the next step due to QC failures.

HABITUATION AND BEHAVIOR TRAINING

In order to reduce stress during the experiment, a 2-week+ training procedure was used to 1) habituate mice to extended periods of head-fixation on the running wheel, and 2) pre-expose mice to the entire set of visual stimuli included in the experimental dataset.

Habituation Rig Design

Mice were habituated in individual sound-attenuating enclosures arranged in clusters (**Figure 8**). Each enclosure contained a behavior stage in a geometry identical to that of the Neuropixels rigs. A 24" LCD monitor was positioned 15 cm from the mouse's right eye, with the sagittal axis of the head parallel to the screen. A registered headframe clamp was attached to a behavior stage equipped with kinematic mounts to ensure repeatable placement of the stage in the enclosure. Enclosures were equipped with a camera coupled with IR illumination to monitor mouse activity.

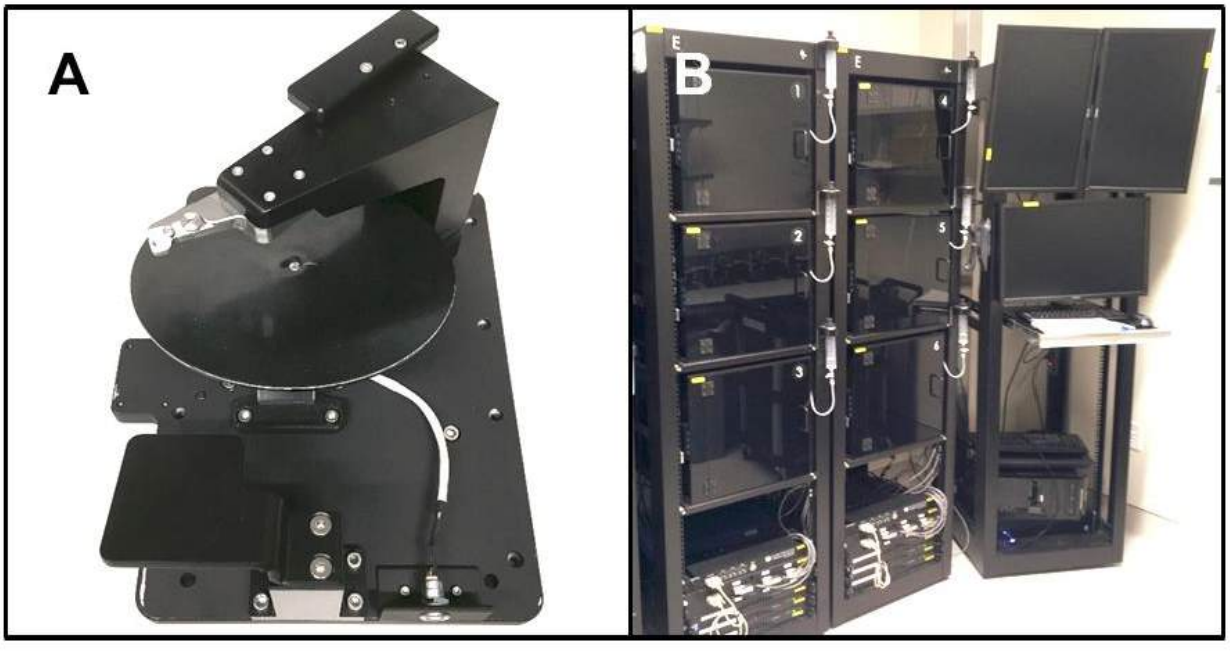

Figure 8. Behavior training platform. (A) Custom behavior stage equipped with a fixed-position headframe clamp and adjustable-height running wheel. The underside of the stage has a kinematic mount plate that mates to the floor of the behavior enclosure allowing reproducible placement of the stage in relationship to the LCD monitor (not shown). (**B)** Behavioral training clusters, allowing multiple mice to be habituated in parallel.

Habituation and Passive Training Procedures

Habituation Phase. Mice were habituated to handling, the behavior stage and enclosure, visual stimuli, and short periods of head-fixation. Habituation was performed for five days:
Days 1-2: Mice were removed from the home cage and gently handled for 1-2 min, then were allowed to explore the behavior stage inside the lit behavior enclosure for 5-8 min.
Days 3-5: Mice were removed from the home cage and handled for 1-2 min, then head-fixed by securing the clamp plate in the behavior stage. The stage was placed in the lit behavior enclosure for 5-8 min. Mice were continuously monitored via webcams.

Passive Training Phase. Passive training was performed to habituate mice to extended periods of head-fixation and expose the mice to the complete stimulus set that would be presented during the recording phase.
Day 6-10: Mice were removed from the home cage and handled for 1-2 min. Mice were then head-fixed to the behavior stage and the stage was placed in the behavior enclosure. A set of full-screen stimuli was displayed for increasing periods ranging from 10 min to 60 min. By the end of this training phase, animals were exposed to the full set of experimental stimuli.

Recording Rig Phase. Mice are habituated to the actual recording rig for two days prior to the actual experiment. The recording rig differs from the behavior boxes in that the enclosed space is much larger, and the protective cone and Neuropixels probe cartridge are visible in the mouse's left visual field (but do not obscure the visual stimulation monitor). The head fixation system and running wheel are identical to what the mouse has been exposed to previously.
Day 11: Mice are head-fixed on the recording rig for 75 minutes, with the probe cartridge lowered to simulate an actual recording. They passively view a truncated version of the same stimulus set that will be shown during the experiment, but with fewer repeats of each stimulus type.
Day 12: Same as Day 11, but with a 100-minute version of the visual stimulus.

Habituation Quality Control

Upon completion of Day 10 of Passive Training mice received an assessment of overall stress level that reflected observations made by the trainer during the entire Habituation and Passive Training phase, including coat appearance,

components of the mouse grimace scale, and overall body movements. Out of 92 mice entering habituation, 2 did not pass on to the insertion window implantation step.

INSERTION WINDOW IMPLANTATION

On the day of recording, the cranial coverslip was removed and replaced with an insertion window containing holes aligned to six cortical visual areas (**Figure 9**). First, the mouse was anesthetized with isoflurane (3%–5% induction and 1.5% maintenance, 100% O_2) and eyes were protected with ocular lubricant (I Drop, VetPLUS). Body temperature was maintained at 37.5°C (TC-1000 temperature controller, CWE, Incorporated). Metabond bridges were removed from the glass cranial window (**Figure 10C**), followed by the sealing layer of Kwik-Cast (**Figure 10D**). Using a 2 mm silicone suction cup, the cranial window was gently lifted to expose the brain (**Figure 10E**). The insertion window was then placed in the headframe well and sealed with Metabond (**Figure 10H**). An agarose mixture was injected underneath the window and allowed to solidify (**Figure 10J**). The mixture consists of 0.4 g high EEO Agarose (Sigma-Aldrich), 0.42 g Certified Low-Melt Agarose (Bio Rad), and 20.5 mL ACSF (135.0 mM NaCl, 5.4 mM KCl, 1.0 mM $MgCl_2$, 1.8 mM $CaCl_2$, 5.0 mM HEPES). This mixture was optimized to be firm enough to stabilize the brain with minimal probe drift, but pliable enough to allow the probes pass through without bending. Finally, a layer of silicone oil (30,000 cSt, Aldrich) was added to prevent the agarose from drying (**Figure 10K**) and a plastic cap was added to the headframe well to keep out cage debris. At the end of this procedure, mice were returned to their home cages for 1-2 hours.

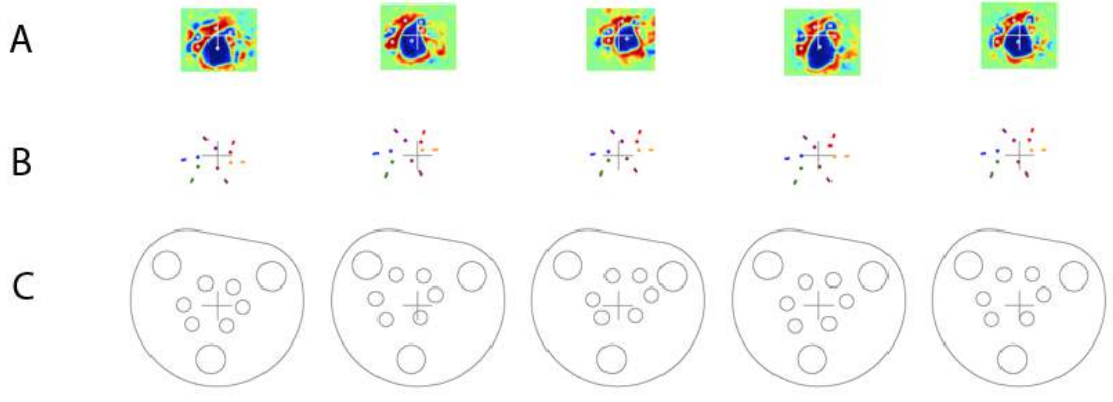

Figure 9. Design of the insertion window. (A) Visual sign maps for 5 mice, automatically generated from the ISI procedure. Cortical visual areas are represented as contiguous blue or red patches. Target points are placed at the retinotopic center of each visual area (except for VISrl, where the target is shifted toward the geometric center). **(B)** The tips of 6 Neuropixels probes are calibrated to the same coordinate system as the ISI rig. Using the computed offset and orientation of each probe from the center of the imaging plane, the intersection between the probe shank and the insertion window can be computed, assuming each probe will enter the brain at the center of one visual area (colored lines). **(C)** An insertion window design is automatically generated for each mouse, with 1 mm diameter holes at the locations required for each probe to reach the desired cortical target. The windows are then laser-cut out of a 0.02” thick clear PETG plastic sheet (Ponoko) for use in the experiment.

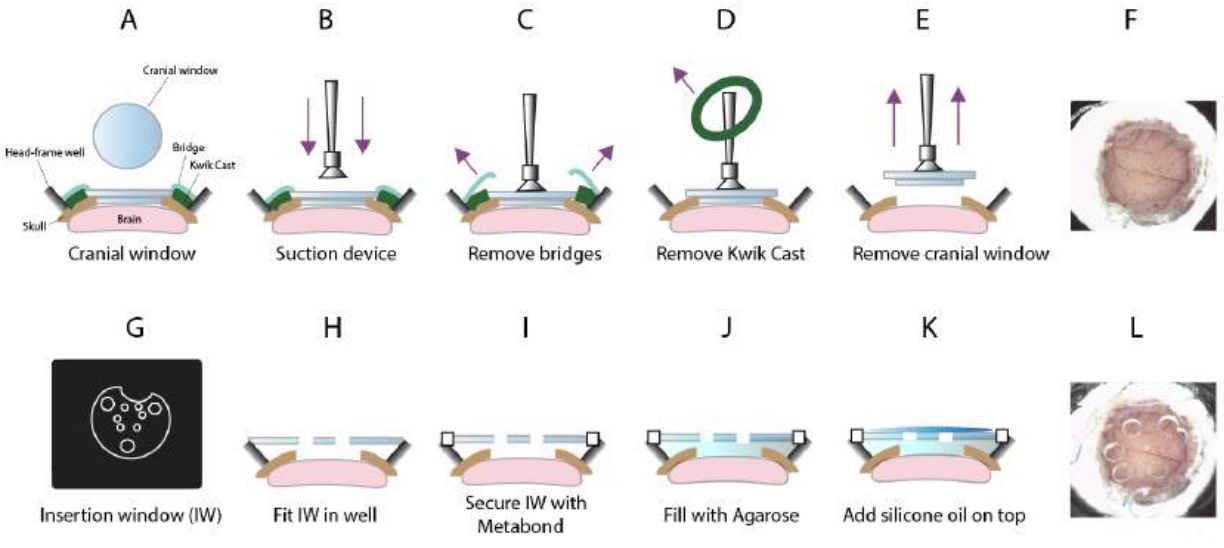

Figure 10. Steps required for insertion window implantation. (A) Cranial window preparation. **(B–F)** The cranial window is freed from the skull, then gently lifted using suction, exposing the brain. **(G)** Example plastic insertion window. **(H–J)** The insertion window is secured to the headframe well, and the empty space between the window and brain is filled with an agarose/ACSF mixture. **(K)** Openings in the plastic window are sealed with silicone oil, to prevent the agarose from drying. **(L)** Final insertion window preparation.

Insertion Window Quality Control

3 out of 90 mice did not pass through to the recording step due to procedure failures during insertion window implantation. These failures were caused by the headframe coming loose from the skull, after which the mice were euthanized.

NEUROPIXELS RECORDINGS

Probes

All recordings were carried out with Neuropixels probes (Jun et al., 2017). These probes are based on the complementary metal-oxide-semiconductor (CMOS) technology used for making silicon integrated circuits. They contain 960 recording sites, a subset of 374 (Neuropixels 3a) or 383 (Neuropixels 1.0) of which can be configured for recording at any given time. The sites are oriented in a “staggered” layout on a 70 μm wide x 10 mm long shank (**Figure 11**). Neural signals are routed to an integrated base containing amplification, digitization, and multiplexing circuitry. The signals from each recording site are split in hardware into a spike band (30 kHz sampling rate, 500 Hz highpass filter) and an LFP band (2.5 kHz sampling rate, 1000 Hz lowpass filter). Due to their dense site configuration (20 μm vertical separation) over a ~3.8 mm span, each probes has the capacity to record hundreds of neurons at the same time. Our goal was to insert 6 probes/mouse. Overall, a penetration success of 5.7 probes/mouse was achieved, with failures due to dura regrowth, collisions with the protective cone or optotagging fiber, or probe breakage during manipulation.

The base of each probes contains 32 10-bit analog-to-digital converters (ADCs), each of which are connected to 12 spike-band channels and 12 LFP-band channels via multiplexers. A full cycle of digitization requires 156 samples: 12 samples from each of 12 spike-band channels, and 1 sample from each of 12 LFP-band channels. Each ADC serves a contiguous bank of odd or even channels, so ADC 1 digitizes channels [1,3,5,...,23], ADC 2 digitizes channels [2,4,6,...,24], ADC 3 digitizes channels [25,27,29,...,47], etc. Because of the need for interleaved sampling, common-mode noise will be shared across all channels that are acquired simultaneously, e.g. [1,2,25,26,49,50,...,361,362].

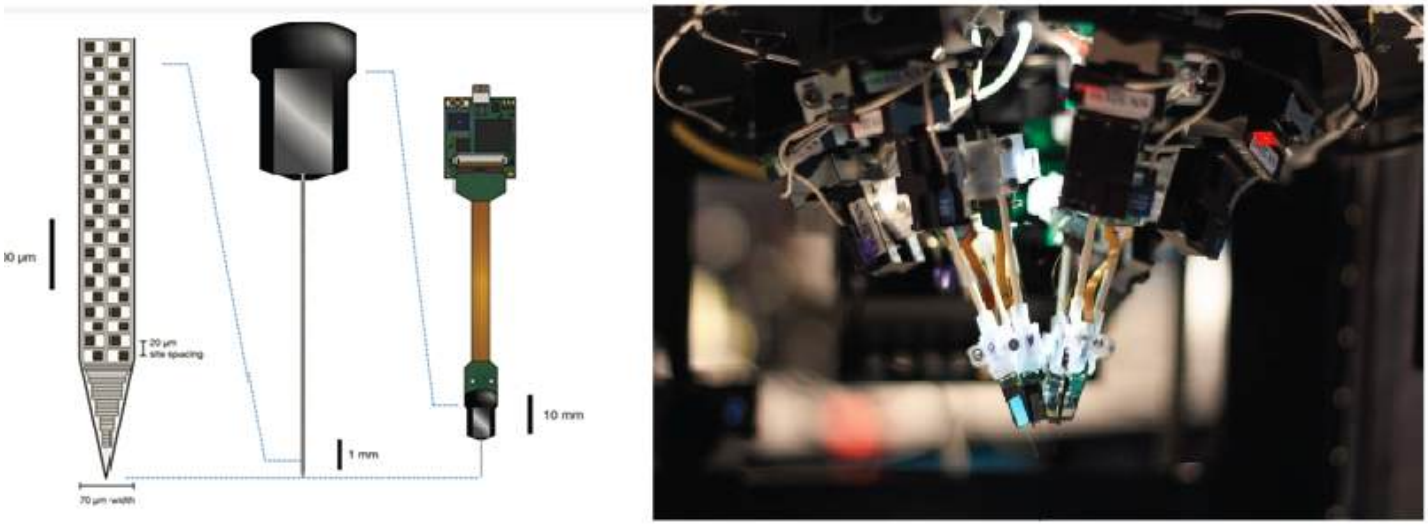

Figure 11. Neuropixels probes. Left: Diagram of the probe at three different zoom levels, showing the recording site layout, the shank and base, and the overall package. Right: Six probes mounted on the recording rig. Each probe is attached to an independent 3-axis manipulator and is angled to fit within a ~5 mm recording window.

Experimental Rig

The experimental rig (**Figure 12**) was designed to allow six Neuropixels probes to penetrate the brain approximately perpendicular to the surface of visual cortex. Each probe is mounted on a 3-axis micromanipulator (New Scale Technologies, Victor, NY), which are in turn mounted on a solid aluminum plate, known as the probe cartridge. The cartridge can be removed from the rig using a pair of pneumatic tool-changers, to facilitate probe replacement and maintenance.

Workflow Sequencing Engine

The experimental procedure is guided by a Work Sequencing Engine (WSE), a custom GUI written in Python. This software ensures that all experimental steps are carried out in the correct order, reducing trial-to-trial variability and optimizing operator efficiency. The GUI logs the operator ID, mouse ID, and session ID, and ensures that all hardware and software are properly configured. The WSE is not only a list of tasks at each stage but is also used to start and stop the visual stimulus, the body and eyetracking cameras, and Neuropixels data acquisition.

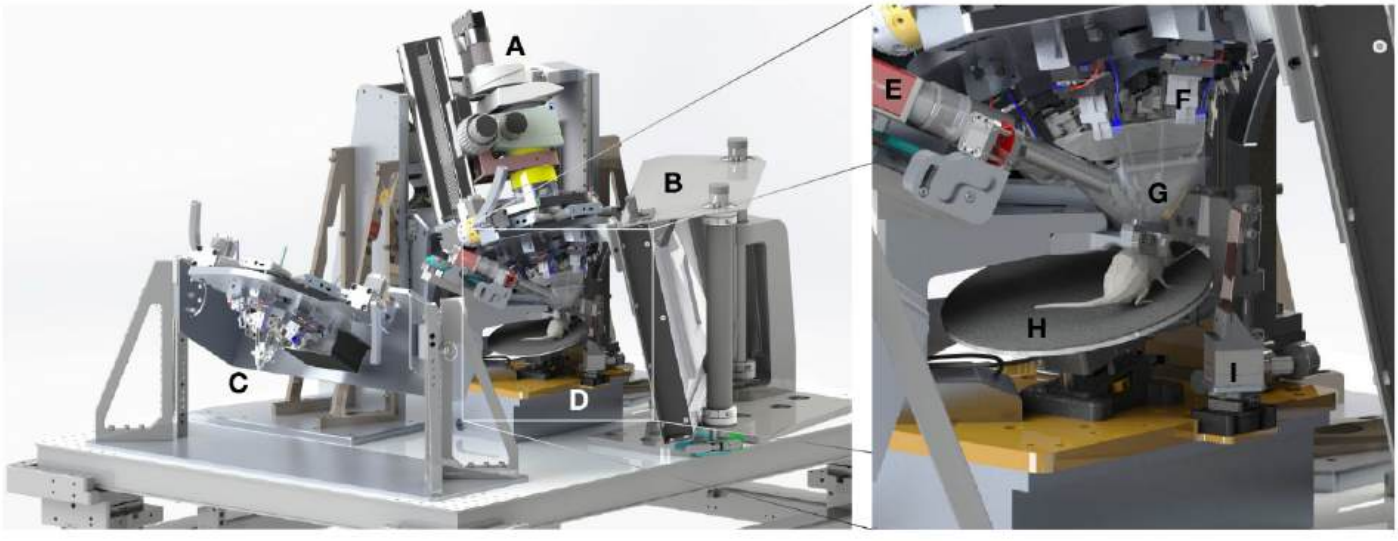

Figure 12. Recording rig. (A), Stereomicroscope used to visualize the insertion site. The eyepieces have been replaced with cameras, to enable remote viewing while the rig is enclosed. **(B)**, Visual stimulus monitor. **(C)**, Maintenance stand used to repair and replace probes, headstages, manipulators, and ground wires. **(D)**, Behavior stage. **(E)**, Eyetracking camera. **(F)**, Manipulators used to align probes with visual areas. **(G)**, Protective cone, to prevent the mouse's tail from contacting the probes. **(H)**, Running wheel. **(I)**, IR dichroic, to reflect the mouse's eye without obscuring the view of the stimulus monitor.

Probe Alignment

The tip of each probe was aligned to its associated opening in the insertion window using a coordinate transformation obtained via a prior calibration procedure. The XY locations of the visual area retinotopic centers were supplied by the Workflow Sequencing Engine (WSE), and these values were translated into XYZ coordinates for each 3-axis manipulator using a custom Python script. The operator then moved each probe into the desired location prior to placing the mouse on the rig.

Application of CM-DiI

Precise localization of Neuropixels probes in the target brain areas cannot be made by electrolytic lesions (current cannot be delivered through the recording sites) or DAPI/Nissl staining of tissue (the probes are too thin to show visible tracks). Instead, CM-DiI (1 mM in ethanol; ThermoFisher Product #V22888) was used because its fluorescence is maintained after brain clearing, and it has a limited diffusion radius. The probes were coated before each recording by immersing them one by one into a well filled with dye (Figure 13). A single dip is sufficient to clearly see the probe tracks in the ex vivo imaging step. At this stage, the probes were checked for collisions. If adjacent probes collide with one another during insertion into the CM-DiI well, they will not be lowered to the maximum depth during the experiment.

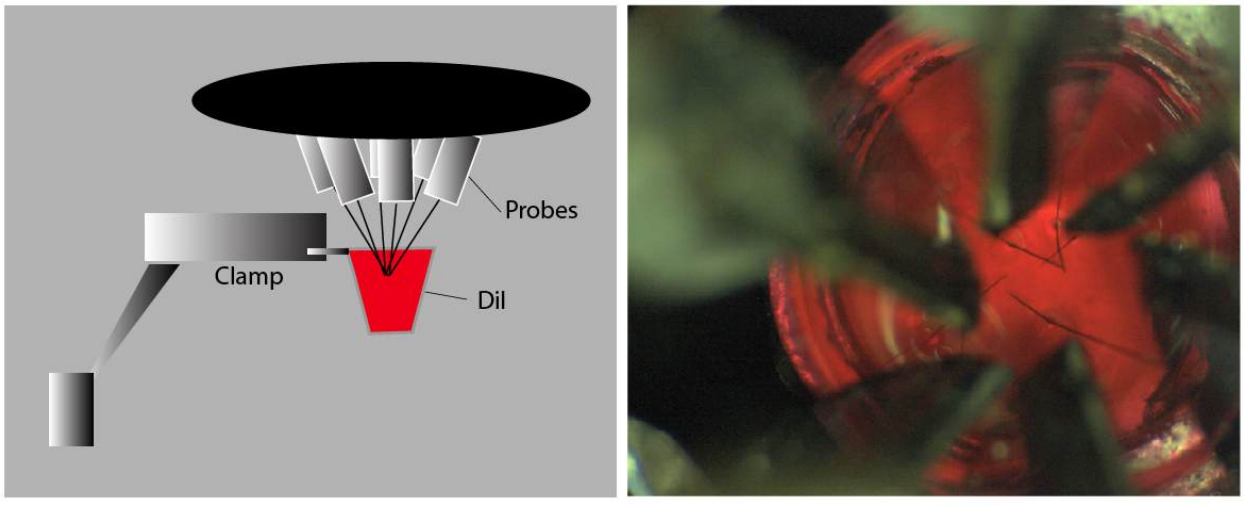

Figure 13. CM-DiI application procedure. Left, Prior to recording, 6 probe shanks are submerged in a bath of CM-DiI to a depth of at least 4 mm. A plastic well was glued to a standard headframe and clamped into the headframe holder. Right, view of the probes in the red dye.

Head Fixation

The mouse was placed on the running wheel and fixed to the headframe holder with three set screws. Next, the plastic cap was removed and an aluminum cone was lowered to prevent the mouse tail from contacting the probes. An IR dichroic mirror was placed in front the right eye to allow the eyetracking camera to operate without interference from the visual stimulus (**Figure 14A**). A black curtain was then lowered over the front of the rig, placing the mice in complete darkness except for the screen.

Grounding

A 32 AWG silver wire (A-M Systems) was cemented to the skull during the headframe/cranial window surgery. This wire becomes electrically conductive with the brain surface following the application of the ACSF/agarose mixture beneath the insertion window. The ground wire was pre-soldered to a gold pin embedded in the headframe well, which mates with a second gold pin on the protective cone (**Figure 14B,C**). The cone pin was soldered to 22 AWG hook-up wire (SparkFun Electronics), which was connected to both the behavior stage and the probe ground (via the pneumatic tool-changer). Prior to the experiment, the brain-to-probe ground path was checked using a multimeter.

The reference connection on the Neuropixels probes was permanently soldered to ground using a silver wire. The headstage grounds (which are contiguous with the Neuropixels probe grounds) were connected together with 36 AWG copper wire (Phoenix Wire). For Neuropixels 3a, two probes had a direct path to animal ground, and the others were wired up serially. All probes were also connected to the mains ground via the data cable (a dual coaxial cable). For Neuropixels 1.0, all probes were connected in parallel to animal ground, and were not connected to the mains ground through the data cable (a single twisted pair cable).

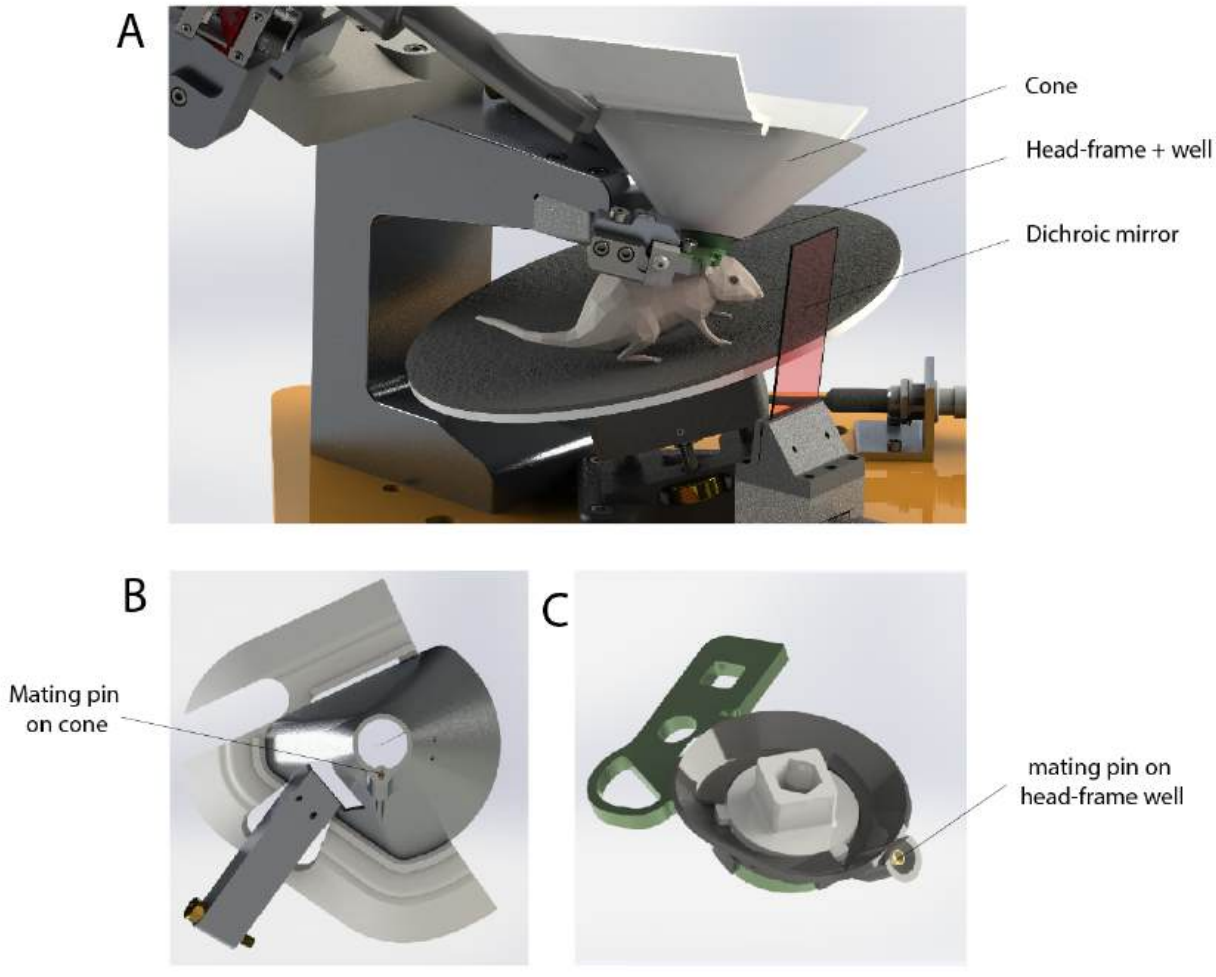

Figure 14. Head fixation and grounding. (A) The mouse is head-fixed while free to run on a wheel. An aluminum cone with 3D-printed wings makes direct contact with the edge of the headframe well to prevent the mouse's tail from interfering with the probes and manipulators. **(B)** The protective cone contains a gold pin that is connected to the probe ground. **(C)** A mating gold pin is embedded in the headframe. This pin is soldered to a silver wire that becomes electrically conductive with the brain surface following application of the agarose/ACSF mixture.

Probe insertion

The probes were initially held on a motorized cartridge approximately 30 cm above the mouse. Once the mouse was in the headframe, the cartridge was lowered so the probe tips were approximately 2.5 mm above the brain surface. The probes were then manually lowered one by one to the brain surface until spikes were visible on the electrodes closest to the tip. This step must be performed manually to watch for probes bending on the insertion window, agarose, or brain surface. After the probes penetrated into the brain to a depth of ~100 microns, they were descended automatically at a rate of 200 µm/min (total of 3.5 mm or less in the brain) to prevent damage caused by rapid insertion (Fiáth et al., 2019). Once the probes reached their targets, they were allowed to settle for 5 to 10 min. Photo-documentation was taken with the probes fully retracted, after the probes reached the brain surface (**Figure 15A**), and after the probes were fully inserted (**Figure 15B**).

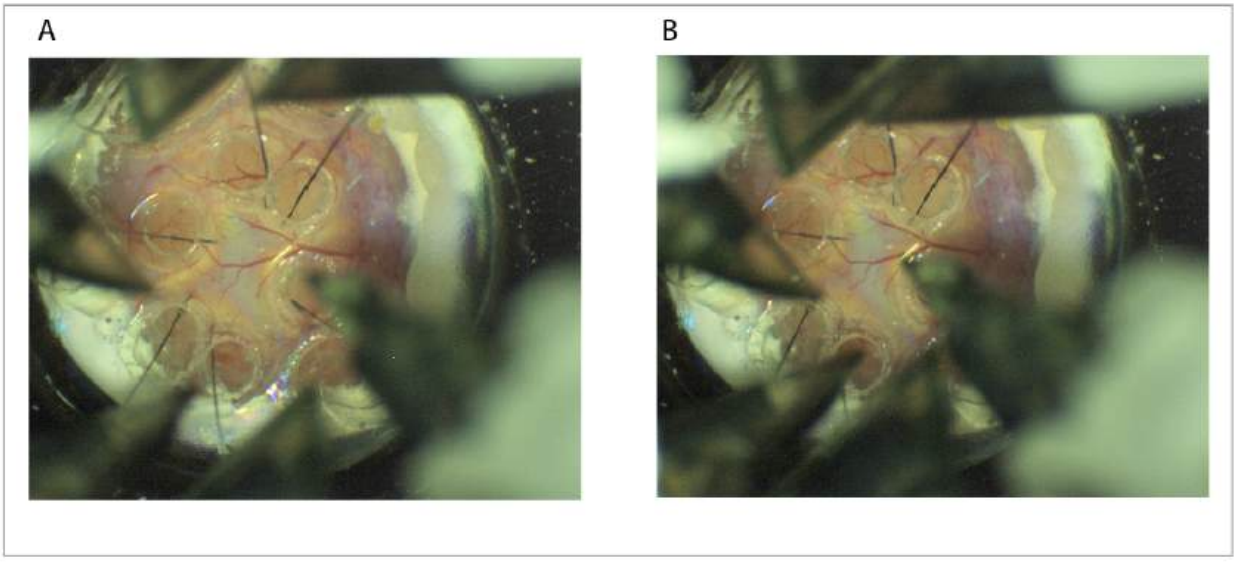

Figure 15. Brain surface photodocumentation. (A) Image acquired after 6 probes have reached the surface of the brain. (**B)** Image acquired after the probes have reached their final depths.

Data acquisition and synchronization

Neuropixels data was acquired at 30 kHz (spike band) and 2.5 kHz (LFP band) using the Open Ephys GUI (Siegle et al., 2017). Gain settings of 500x and 250x were used for the spike band and LFP bands, respectively. Each probe was either connected to a dedicated FPGA (Neuropixels 3a) or a PXIe card inside a National Instruments chassis (Neuropixels 1.0). Raw neural data was streamed to a compressed format for archiving which was extracted prior to analysis.

Videos of the eye and body were acquired at 30 Hz. The angular velocity of the running wheel was recorded at the time of each stimulus frame, at approximately 60 Hz. Synchronization signals for each frame were acquired by a dedicated computer with a National Instruments card acquiring digital inputs at 100 kHz, which was considered the master clock. A 32-bit digital "barcode" was sent with an Arduino Uno (SparkFun DEV-11021) every 30 s to synchronize all devices with the neural data. Each Neuropixels probe has an independent sample rate between 29,999.90 Hz and 30,000.31 Hz, making it necessary to align the samples offline to achieve precise synchronization. The synchronization procedure used the first matching barcode between each probe and the master clock to determine the clock offset, and the last matching barcode to determine the clock scaling factor. If probe data acquisition was interrupted at any point during the experiment, each contiguous chunk of data was aligned separately. Because one LFP band sample was always acquired after every 12^{th} spike band sample, these data streams could be synchronized automatically once the spike band clock rate has been determined.

To synchronize the visual stimulus to the master clock, a silicon photodiode (PDA36A, Thorlabs) was placed on the stimulus monitor above a "sync square" that flips from black to white every 60 frames. The analog photodiode signal is thresholded and recorded as a digital event by the sync computer. Individual frame times are reconstructed by interpolating between the photodiode on/off events.

Stimulus monitor

Visual stimuli were generated using custom scripts based on PsychoPy (Peirce, 2007) and were displayed using an ASUS PA248Q LCD monitor, with 1920 x 1200 pixels (21.93 in wide, 60 Hz refresh rate). Stimuli were presented monocularly, and the monitor was positioned 15 cm from the mouse's right eye and spanned 120° x 95° of visual space prior to stimulus warping. Each monitor was gamma corrected and had a mean luminance of 50 cd/m^2. To account for the close viewing angle of the mouse, a spherical warping was applied to all stimuli to ensure that the apparent size, speed, and spatial frequency were constant across the monitor as seen from the mouse's perspective (**Figure 16**).

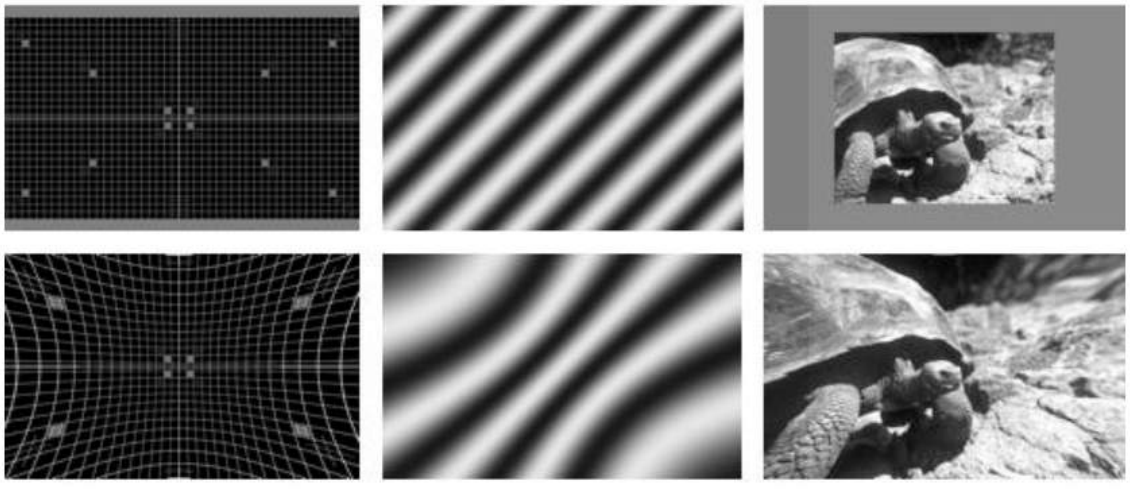

Figure 16. Demonstration of stimulus warping. Top, unwarped images, bottom, warped images.

Visual Stimuli

All experiments began with a receptive field mapping stimulus consisting of 2 Hz, 0.04 cycles per degree drifting gratings with a 20º circular mask. These Gabor patches randomly appeared at one of 81 locations on the screen (9 x 9 grid) for 250 ms at a time, with no blank interval. The receptive field mapping stimulus was followed by a series of dark or light full-field flashes, lasting 250 ms each and separated by a 2 second inter-trial interval.

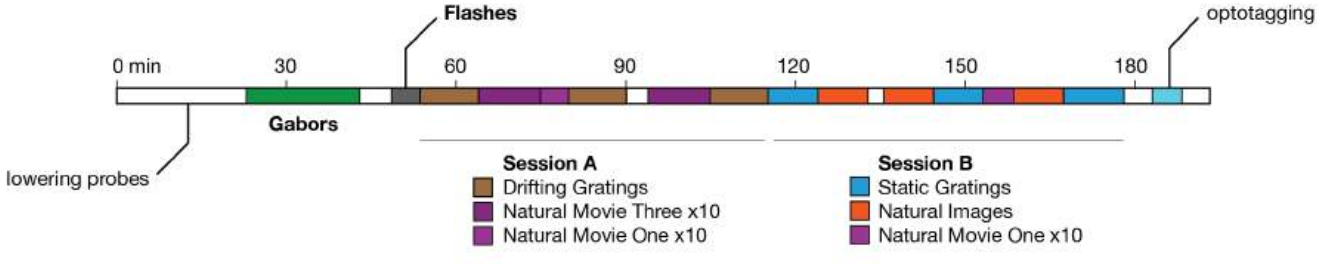

Figure 17. "Brain Observatory 1.1" visual stimulus set. Colors indicate the timing of each stimulus block (white = mean luminance blank screen).

Next, mice were shown one of two possible stimulus sets. The first, called "Brain Observatory 1.1" is a concatenation of two sessions from the Two-Photon Imaging Brain Observatory (de Vries et al., 2018). Drifting gratings were shown with a spatial frequency of 0.04 cycles/deg, 80% contrast, 8 directions (0º, 45º, 90º, 135º, 180º, 225º, 270º, 315º, clockwise from 0º = right-to-left) and 5 temporal frequencies (1, 2, 4, 8, and 15 Hz), with 15 repeats per condition. Static gratings were shown at 6 different orientations (0º, 30º, 60º, 90º, 120º, 150º, clockwise from 0º = vertical), 5 spatial frequencies (0.02, 0.04, 0.08, 0.16, 0.32 cycles/degree), and 4 phases (0, 0.25, 0.5, 0.75); they are presented for 0.25 seconds, with no intervening gray period. The Natural Images stimulus consisted of 118 natural images taken from the Berkeley Segmentation Dataset (Martin et al., 2001), the van Hateren Natural Image Dataset (van Hateren and van der Schaaf, 1998), and the McGill Calibrated Colour Image Database (Olmos and Kingdom, 2004). The images were presented in grayscale and were contrast normalized and resized to 1174 x 918 pixels. The images were presented in a random order for 0.25 seconds each, with no intervening gray period. Two natural movie clips were taken from the opening scene of the movie Touch of Evil (Welles, 1958). Natural Movie One was a 30 second clips repeated 20 times (2 blocks of 10), while Natural Movie Three was a 120 second clip repeated 10 times (2 blocks of 5). Natural Movie Two from the original

Brain Observatory stimulus set was not shown. All clips were contrast normalized and were presented in grayscale at 30 fps.

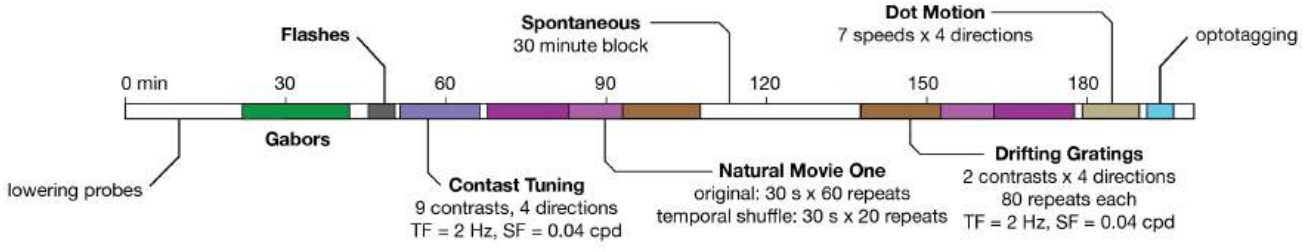

Figure 18. "Functional Connectivity" visual stimulus set. Colors indicate the timing of each stimulus block (white = mean luminance blank screen).

The second stimulus set, called "Functional Connectivity," consisted of a subset of the stimuli from the Brain Observatory set shown with a higher number of repeats. Drifting gratings were presented at 4 orientations and one temporal frequency (2 Hz) with 75 repeats. A contrast-tuning stimulus consisting of drifting gratings at 4 directions (0º, 45º, 90º, 135º, clockwise from 0º = left-to-right) and 9 contrasts (0.01, 0.02, 0.04, 0.08, 0.13, 0.2, 0.35, 0.6, 1.0) was also shown. The Natural Movie One stimulus was presented a total of 60 times, with an additional 20 repeats of a temporally shuffled version. Last, a dot motion stimulus consisting of approximately 200 1.5º radius white dots on a mean-luminance gray background moving at one of 7 speeds (0º/s, 16º/s, 32º/s, 64º/s, 128º/s, 256º/s, 512º/s) in four different directions (0º, 45º, 90º, 135º, clockwise from 0º = left-to-right) at 90% coherence was shown.

The data cube (genotypes x areas x stimuli) for the publicly available dataset is shown in **Table 1**.

Genotype	Stimulus Set	VISp	VISl	VISal	VISpm	VISam	VISrl	LGd	LP	CA1	CA3	DG
Wild type	Brain Observatory 1.1	16	12	11	9	11	15	12	10	12	12	12
	Functional Connectivity	13	8	12	9	13	12	9	14	14	14	14
Sst-IRES-Cre;Ai32	Brain Observatory 1.1	6	3	4	5	6	5	3	5	5	4	5
	Functional Connectivity	6	4	5	4	6	6	1	4	6	5	6
Pvalb-IRES-Cre;Ai32	Brain Observatory 1.1	5	4	5	3	4	4	3	3	5	5	4
	Functional Connectivity	3	3	2	2	3	2	1	1	3	3	3
Vip-IRES-Cre; Ai32	Brain Observatory 1.1	5	5	4	3	5	4	3	4	4	4	4
	Functional Connectivity	2	3	1	1	2	2	2	3	3	3	3

Table 1. The Visual Coding Neuropixels Data Cube. Each experiment is performed on a mouse of one of four genotypes (wt, Sst, Pvalb, Vip), and uses one of two stimulus sets (Brain Observatory 1.1 or Functional Connectivity). However, multiple regions can be recorded in one experiment. The total number of recordings per area for each genotype x stimulus combination are shown here.

Optotagging

After the visual stimulus was finished, the same optotagging procedure was carried out on all mice, regardless of genotype. Blue light was delivered by a 465 nm LED (Plexon) controlled by a Cyclops LED driver (Newman et al., 2015) or a 473 nm laser (Laser Quantum, model ciel or Cobolt model 06-MLD). The light source was coupled to a 400 μm diameter fiber optic cable (Thorlabs), with the tip positioned such that blue light illuminated the entire cranial window. Four types of stimuli at 3 different light levels were randomly interleaved: 2 ms pulses at 10 Hz, one 5 ms pulse, one 10 ms pulse, or a 1s raised cosine ramp. Stimuli were presented at intervals of 1.5 s plus a uniformly distributed delay between 0 and 0.5 s. Mice were had no exposure to the optotagging stimulus prior to the end of the recording session.

Probe Removal and Cleaning

Probes were retracted from the brain at a rate of 1 mm/s, after which the probe cartridge was lifted up to its full height. The 3D-printed protective cap was screwed into the headframe well, then mice were removed from head fixation and returned to their home cages overnight. Probes were immersed in a well of 1% Tergazyme overnight, which was sufficient to remove tissue and silicone oil prior to the next day's recording session.

Neuropixels Recording Quality Control

A total of 87 mice entered the recording step, with 26 QC failures due to: white foam buildup on the edge of the eye partially covering the pupil (8 mice); bleeding on the cortical surface obscuring the vasculature (4 mice); fewer than four probes successfully inserted into the brain (1 mouse); software failures (3 mice); high RMS noise levels in the spike band (4 mice); or probe drift (6 mice). In total, 61 mice passed all QC criteria and passed to the *ex vivo* imaging step.

Invalid intervals

Occasionally, there were problems with data acquisition that did not warrant failing the entire experiment, but did cause a portion of the data to be marked as invalid.

Stimulus failures. Frames that remained on the screen for >3x the standard frame duration (50 ms) invalidated the stimulus for at least 1 s before and after the long frames. This occurred in 7 sessions, for a total of 312 s of invalid data across all probes (out of a possible 64,260 s).

Data loss for one probe. The firmware buffer on an individual Neuropixels 3a probe sometimes overflowed, requiring that probe's data acquisition to be re-started in the middle of an experiment. This occurred for 15 probes across 13 sessions, for a total of 8650 s of invalid data for individual probes (out of a possible 716,040 s).

Gain fluctuations. There was an issue with Neuropixels 1.0 probes that caused the spike band gain of all probes to simultaneously drop to 0, and return to normal over the course of ~1 s. Saturating events in the LFP band co-occurred with these gain fluctuations. These fluctuations were detected in 2 sessions, for a total of 98.5 s of invalid data across all probes (out of a possible 18,360 s).

EX VIVO IMAGING

Tissue Clearing

Mice were perfused with 4% PFA (after induction with 5% isoflurane and 1 L/min of O_2). The brains were preserved in 4% PFA, rinsed with 1x PBS the next morning, and stored at 4°C in PBS. Next, brains were run through a tissue clearing process based on the iDISCO method (Renier et al., 2014). This procedure uses different solvents which dehydrate and delipidate the tissue. The first day, the brains were immersed in different concentrations of methanol (20, 40, 60) for an hour each, then overnight in 80% methanol. On the second day, they were dipped into 100% methanol (twice for one hour) and then into a mixture of 1/3 methanol and 2/3 dichloromethane overnight. Finally, on the third day, the brains were

moved from pure dichloromethane (2 x 20 min) to pure dibenzyl ether, where they remained for 2 days until clearing was complete (**Figure 19**).

Figure 19. Brain after the tissue clearing. The brain becomes slightly yellow and very firm after the final clearing step.

Optical Projection Tomography (OPT)

Whole-brain 3D imaging was accomplished with optical projection tomography (OPT) (Nguyen et al., 2017; Sharpe, 2002; Wong et al., 2013). The OPT instrument consisted of collimated light sources for transmitted illumination (on-axis white LED, Thorlabs MNWHL4 with Thorlabs SM2F32-A lens and Thorlabs DG20-600 diffuser) or fluorescence excitation (off-axis Thorlabs M530L3, with Thorlabs ACL2520U-DG6-A lens and Chroma ET535/70m-2P diffuser), a 0.5x telecentric lens (Edmund Optics 62-932) with emission filter (575 nm LP, Edmund Optics 64-635), and a camera (IDS UI-3280CP). The specimen was mounted on a rotating magnetic chuck attached to a stepper motor, which positioned the specimen on the optical axis and within a glass cuvette filled with dibenzyl ether. The stepper motor and illumination triggering were controlled with an Arduino Uno (SparkFun DEV-11021) and custom shield including a Big Easy Driver (SparkFun ROB-12859). Instrument communication and image capture was accomplished with MicroManager (Edelstein et al., 2014).

A series of 400 images were captured with transmitted LED illumination with each image captured with the specimen rotated 0.9 degrees relative to the previous position. This series of 400 images was repeated with the fluorescence excitation LED. Each channel was stored as a separate OME-TIFF stack before extracting individual planes and metadata required for reconstruction using a custom Python script.

Isotropic 3D volumes were reconstructed from these projection images using NRecon (Bruker). The rotation axis offset and region-of-interest bounds were set for each image series pair using the transmitted channel dataset, then the same values applied to the fluorescence channel dataset. A smoothing level of 3 using a Gaussian kernel was applied to all images. Reconstructions were exported as single-plane 16-bit TIFF images taken along the rotation axis with final voxel size of 7.9 μm per side.

Registering Probes to the Common Coordinate Framework

Reconstructed brains were downsampled to 10 μm per voxel and roughly aligned to the Allen Institute Common Coordinate Framework (CCFv3) template brain using an affine transform. The volume was then cropped to a size of 1023 x 1024 x 1024 and converted to Drishti format (http://sf.anu.edu.au/Vizlab/drishti). Next, 6-54 registration points were marked in up to 14 coronal slices of the individual brain by comparing to the CCFv3 template brain (**Figure 20A**). Fluorescent probe tracks were manually labeled in coronal slices of the individual brain, and the best-fit line was found using singular value decomposition (**Figure 20B**). The registration points were used to define a 3D nonlinear transform (VTK thinPlateSplineTransform), which was used translate each point along the probe track into the CCFv3 coordinate space. Each CCFv3 coordinate corresponds to a unique brain region, identified by its structure acronym (e.g., CA3, LP, VISp, etc.). A list of CCFv3 structure acronyms along each track was compared to the physiological features measured by each probe (e.g., unit density, LFP theta power). The location of major structural boundaries were manually adjusted

to align the CCFv3 labels with the physiology data, and each recording channel was assigned to a CCFv3 structure. In this way, each channel could be mapped to a unique brain region.

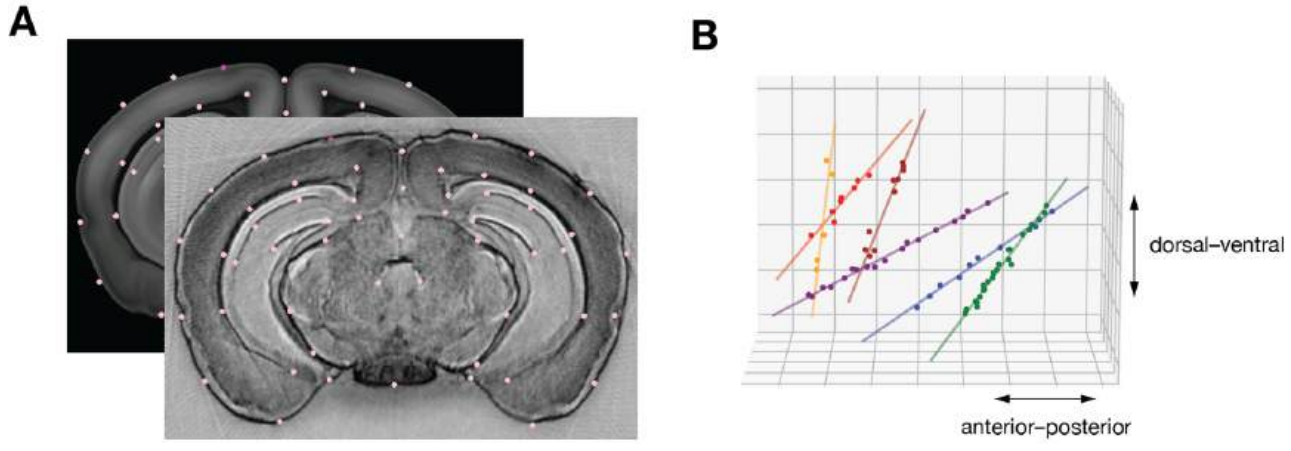

Figure 20. Summary of CCF registration methods. (A) Registration points from the CCFv3 template brain (rear) are manually marked on each individual brain using custom software (front). Most of the points lie at the borders between brain regions, such as thalamus and hippocampus or hippocampus and cortex. **(B)** Dots represent the extracted 3D coordinates of each of 6 probes, with the best-fit line overlaid. Points along the best-fit line are translated into CCFv3 space using the transform defined from the registration points in (A).

Identification of cortical visual area targets

To confirm the identity of the cortical visual areas, images of the probes taken during the experiment were compared to images of the brain surface vasculature taken during the ISI imaging session. Based on the vasculature patterns, the ISI map was overlapped with the insertion photodoc image. When done in custom software, key points were selected along the vasculature on both images and a perspective transform (OpenCV) was performed to warp the insertion image to the ISI target image. When done manually, the key points of the vasculature were selected as well but the overlap of both images was done in Photoshop or Illustrator (Adobe Suite). In both cases the probe entry points were manually annotated. Finally, an area was assigned to each probe. Overall, successful targeting of the 6 target visual areas occurred at the following rates: 89% for AM, 72% for PM, 98% for V1, 85% for LM, 79% for AL, and 90% for RL. A small subset of penetrations were mapped to LI, MMA, or MMP. Penetration targets that could not be unambiguously associated with a particular visual area were classified as “VIS.” If the cortical area label obtained via CCFv3 registration did not match the area identified via the ISI map overlay, the information in the ISI map took precedence.

DATA ANALYSIS

SPIKE SORTING

Data pre-processing

Data was written to disk in a format containing the original 10-bit samples from each ADC. These files were backed up to a tape drive, then extracted to a new set of files that represent each sample as a 16-bit integer, scaled to account for the gain settings on each channel. Separate data files were generated for the LFP band and spike band, along with additional files containing the times of synchronization events. The extracted files consume approximately 36% more disk space than the originals.

Prior to spike sorting, the spike-band data passed through 4 steps: offset removal, median subtraction, filtering, and whitening. First, the median value of each channel was subtracted to center the signals around zero. Next, the median

across channels was subtracted to remove common-mode noise. While Neuropixels have been measured to have a spike-band RMS noise levels of 5.1 μV in saline (Jun et al., 2017), this cannot be achieved in practice when recording in vivo. The signals become contaminated by background noise in neural tissue; movement artifacts associated with animal locomotion, whisking, and grooming; and electrical noise introduced by the additional wiring required to support multiple probes on one rig. To remove noise sources that are shared across channels, the median was calculated across channels that are sampled simultaneously, leaving out adjacent (even/odd) channels that are likely measuring the same spike waveforms, as well as reference channels that contain no signal. For each sample, the median value of channels N:24:384, where N = [1,2,3,…,24], was calculated, and this value was subtracted from the same set of channels. This method rejects high-frequency noise more effectively than subtracting the median of all channels, at the cost of leaving a residual of ~2 μV for large spikes, visible in the mean waveforms. Given that this value is well below the RMS noise level of the Neuropixels probes under ideal conditions, it should not affect spike sorting. The original data is over-written with the median-subtracted version, with the median value of each block of 16 channels saved separately, to allow reconstruction of the original signal if necessary. The median-subtracted data file is sent to the Kilosort2 Matlab package (https://github.com/mouseland/kilosort2, commit 2fba667359dbddbb0e52e67fa848f197e44cf5ef, April 8, 2019), which applies a 150 Hz high-pass filter, followed by whitening in blocks of 32 channels. The filtered, whitened data is saved to a separate file for the spike sorting step.

Kilosort2

Kilosort2 was used to identify spike times and assign spikes to individual units (Stringer et al., 2019). Traditional spike sorting techniques extract snippets of the original signal and perform a clustering operation after projecting these snippets into a lower-dimensional feature space. In contrast, Kilosort2 attempts to model the complete dataset as a sum of spike "templates." The shape and locations of each template is iteratively refined until the data can be accurately reconstructed from a set of *N* templates at *M* spike times, with each individual template scaled by an amplitude, *a*. A critical feature of Kilosort2 is that it allows templates to be shifted in space as well as time, to account for the motion of neurons relative to the probe over the course of the experiment. Stabilizing the brain using an agarose-filled plastic window has virtually eliminated probe motion associated with animal running, but slow drift of the probe over ~3-hour experiments is still observed. Kilosort2 is able to accurately track units as they move along the probe axis, eliminating the need for the manual merging step that was required with the original version of Kilosort (Pachitariu et al., 2016). The spike-sorting step runs in approximately real time (~3 hours per session) using a dual-processor Intel 4-core, 2.6 GHz workstation with an NVIDIA GTX 1070 GPU.

Parameter	Value
Th	[10 4]
fshigh	150
minfr_goodchannels	0.1
lam	10
AUCsplit	0.9
minFR	1/50
momentum	[20 400]
sigmaMask	30
ThPre	8

Table 2. Kilosort2 parameter values.

Removing putative double-counted spikes

The Kilosort2 algorithm will occasionally fit a template to the residual left behind after another template has been subtracted from the original data, resulting in double-counted spikes. This can create the appearance of an artificially high number of ISI violations for one unit or artificially high zero-time-lag synchrony between nearby units. To eliminate the possibility that this artificial synchrony will contaminate data analysis, the outputs of Kilosort2 are post-processed to remove spikes with peak times within 5 samples (0.16 ms) and peak waveforms within 5 channels (~50 microns). This

process removes >10 within-unit overlapping spikes from 2.5 ± 1.8% of units per session, and 2.05 ± 0.65% of spikes overall.

Removing "noise" units

Kilosort2 generates templates of a fixed length (2 ms) that matches the time course of an extracellularly detected spike waveform. However, there are no constraints on template shape, which means that the algorithm often fits templates to voltage fluctuations with characteristics that could not physically result from the current flow associated with an action potential. The units associated with these templates are considered noise, and are automatically filtered out based on 3 criteria: spread (single channel, or >25 channels), shape (no peak and trough, based on wavelet decomposition), or multiple spatial peaks (waveforms are non-localized along the probe axis). The automated algorithm removed 94% of noise units, or 26% of total units. A final manual inspection step was used to remove an additional 2140 noise units.

LFP PROCESSING

LFP data was downsampled in space by removing 3 out of every 4 channels, leaving channels with 40 μm vertical spacing along the edge of the probe. The data was then downsampled in time from 2.5 kHz to 1.25 kHz after applying a decimation filter (scipy.signal.decimate).

WAVEFORM METRICS

A variety of metrics were computed based on the mean waveform for each unit. Mean waveforms were computed by averaging all channels for 82-sample (2.7 ms) snippets of data around 1000 randomly selected spikes for each unit. The peak of each spike was centered around 20 samples (0.6 ms) from the start of the waveform. Single-channel waveform metrics were computed from a 2.4x upsampled version of the original waveform.

Waveform amplitude: The difference (in microvolts) between the peak and trough of the waveform on a single channel.

Waveform spread: Spatial extent (in microns) of channels where the waveform amplitude exceeds 12% of the peak amplitude.

Waveform duration: Difference (in ms) of the time of the waveform peak and trough on the channel with maximum amplitude.

Signal-to-noise ratio (SNR): After selecting 1000 individual spike waveforms on the channel with maximum amplitude, the mean waveform on that channel was subtracted. SNR is defined the ratio between the waveform amplitude and 2x the standard deviation of the residual waveforms.

SORTING QUALITY METRICS

Overall firing rate: N/T, where N = number of spikes in the complete session and T = total time of the recording session in seconds.

Presence ratio: The session was divided into 100 equal-sized blocks; the presence ratio is defined as the fraction of blocks that include 1 or more spikes from a particular unit. Units with a low presence ratio are likely to have drifted out of the recording, or could not be tracked by Kilosort2 for the duration of the experiment.

Maximum drift: The peak channel was calculated from the top principal component of each individual waveform. The maximum drift is defined as the maximum range of the median peak channel within 51 s intervals equally spaced throughout the session (assuming at least 10 spikes per interval). The average maximum drift across all units is used to identify sessions with a high amount of probe motion relative to the brain.

Silhouette score: A standard metric of cluster quality. It is computed by performing a pairwise comparison between the PCs of the cluster of interest and the PCs of all other units with overlapping channels. The function returns the minimum silhouette score across all pairs (between –1 and 1, with 1 indicating perfect isolation). The scikit-learn implementation of silhouette score was used (Pedregosa et al., 2012).

Inter-spike-interval (ISI) violations: This metric searches for refractory period violations that indicate a unit contains spikes from multiple neurons. The ISI violations metric represents the relative firing rate of contaminating spikes. It is calculated by counting the number of violations <1.5 ms, dividing by the amount of time for potential violations surrounding each spike, and normalizing by the overall spike rate. It is always positive (or 0), but has no upper bound. See (Hill et al., 2011) for more details.

Amplitude cutoff: This metric provides an approximation of a unit's false negative rate. First, a histogram of spike amplitudes is created, and the height of the histogram at the minimum amplitude is extracted. The percentage of spikes above the equivalent amplitude on the opposite side of the histogram peak is then calculated. If the minimum amplitude is equivalent to the histogram peak, the amplitude cutoff is set to 0.5 (indicating a high likelihood that >50% of spikes are missing). This metric assumes a symmetrical distribution of amplitudes and no drift, so it will not necessarily reflect the true false negative rate. But it is still useful for filtering out units that are likely to be missing spikes.

Isolation distance & L-ratio: Take the center of the cluster in PC space and compute the Mahalanobis distance squared required to find the same number of "other" spikes as the total number of spikes for the unit. The better the cluster quality, the higher the isolation distance. L-ratio is the sum of (1 - the chi^2 CDF) for the number of "other" spikes within the isolation distance sphere, divided by the total number of "other" spikes. See (Schmitzer-Torbert et al., 2005) for more information.

d-prime: Linear discriminant analysis is used to find the line of maximum separation in PC space. d-prime indicates the separability of the unit of interest from all other units. See (Hill et al., 2011) for more information.

Nearest neighbors: For each spike belonging to the unit of interest, the four nearest spikes in principal-component space are identified. The "hit rate" is defined as the fraction of these spikes that belong to the unit of interest. The "miss rate" is the fraction of spikes from other units that have their nearest neighbors belonging to the unit of interest. This metric is based on the "isolation" metric from (Chung et al., 2017).

STIMULUS METRICS

Metrics computed for all stimuli

Peri-stimulus firing rate: N/T, N = number of spikes in the stimulus interval, T = time of the stimulus interval in seconds (including blank periods).

Preferred condition: Out of all stimulus conditions (e.g. image, temporal frequency x direction combo, etc.), which one generated the most spikes on average? The blank condition is excluded from this calculation.

Fano factor: The variance of spike rate across trials divided by the mean spike rate across trials, for the preferred condition.

Running modulation: The mean running speed of the mouse was computed for each grating presentation. To calculate the running modulation, the presentations of the preferred grating condition (peak direction and temporal frequency) were broken into "stationary" trials (those when the speed was less than 1 cm/s) and "running" trials (those when the speed was greater than 1 cm/s). Provided that there were at least 10% of trials in each condition, the running modulation was defined as:

$$run_{mod} = C \times \frac{R_{max} - R_{min}}{|R_{min}|}$$

where R_{max} is the larger of the response when the mouse is running or when the mouse is stationary, and R_{min} is the smaller of the two. If R_{max} is the response when the mouse is running, $C = 1$. If R_{max} is the response when the mouse is stationary, $C = -1$.

Drifting gratings

Global orientation selectivity index (gOSI):

$$gOSI = \frac{\sum R_\theta e^{2i\theta}}{\sum R_\theta}$$

where R_θ is the mean response to grating at direction θ at the preferred spatial frequency.

Global direction selectivity index (gDSI):

$$gDSI = \frac{\sum R_\theta e^{i\theta}}{\sum R_\theta}$$

where R_θ is the mean response to grating at direction θ at the preferred spatial frequency.

Modulation index: The stimulus modulation index reflects how spiking activity of each unit is modulated by the temporal frequency of the drifting grating stimulus (Matteucci et al., 2019; Wypych et al., 2012). It is defined as:

$$\left| \frac{\mathrm{PS}\left(\mathrm{f}_{\mathrm{pref}}\right) - \langle \mathrm{PS} \rangle_{\mathrm{f}}}{\sqrt{\langle \mathrm{PS}^2 \rangle_{\mathrm{f}-} \langle \mathrm{PS} \rangle_{\mathrm{f}}^2}} \right|$$

where PS indicates the power spectral density of the peristimulus time histogram (PSTH), and denotes the averaged power over all frequencies. is the preferred temporal frequency of the unit. This metric measures the difference between spiking response power at each unit's preferred frequency and the total power in units of its SDs. The power spectrum was computed using Welch's method to 10 ms-binned PSTH at its preferred condition.

Preferred orientation: The grating orientation that evokes the highest mean firing rate (averaging over temporal frequency).

Preferred temporal frequency: The grating temporal frequency that evokes the highest mean firing rate (averaging over orientation).

Drifting gratings (contrast tuning)

C50: The contrast that evokes 50% of the maximum firing rate, after fitting with a sigmoid curve.

Static gratings

Global orientation selectivity index (gOSI):

$$gOSI = \frac{\sum R_\theta e^{2i\theta}}{\sum R_\theta}$$

where $R\theta$ is the mean response to grating at direction θ at the preferred spatial frequency.

Preferred orientation: The stimulus orientation that evokes the highest mean firing rate (averaging over phase and spatial frequency).

Preferred phase: The stimulus phase that evokes the highest mean firing rate (averaging over orientation and spatial frequency).

Preferred spatial frequency: The stimulus spatial frequency that evokes the highest mean firing rate (averaging over phase and orientation).

Flashes

On/Off ratio: The mean firing rate in response to the "on" (white) flashes divided by the mean firing rate in response to the "off" (black) flashes.

Dot motion

Preferred direction: The stimulus direction that evokes the highest mean firing rate (averaging over speed).

Preferred speed: The stimulus speed that evokes the highest mean firing rate (averaging over direction).

Natural scenes

Image selectivity index: To quantify how selective a cell is for images, the image selectivity was quantified using the following method (Quian Quiroga et al., 2007). The number of responses above a threshold, *T*, is computed as:

$$R(T) = \frac{1}{N}\sum_{i=1}^{N}\theta(f_i - T)$$

where f_i is the response of the neuron to image *i*, *N* is the number of images. *R(T)* is calculated for *M* = 1000 threshold values, evenly spaced between the minimum and maximum responses:

$$T_j = f_{min} + j\frac{f_{max} - f_{min}}{M}$$

The area beneath the curve *R*(*T*) is calculated as:

$$A = \frac{1}{M}\sum_{j=1}^{M}R(T_j)$$

The image selectivity is

$$S = 1 - 2A$$

such that a uniformly responsive cell has a selectivity *S* = 0, while a cell that responds to only one image has a selectivity *S* = 1.

Receptive field mapping

Receptive field: The receptive field for one unit is defined as the 2D histogram of spike counts at each of 81 locations of the Gabor stimulus (9 x 9 matrix).

p_value: A chi-square test for independence was used to assess the presence of a significant receptive field. A chi-square test statistic was computed $\chi^2 = \sum_{i=0}^{n} \frac{(E_i - O_i)^2}{E_i}$, where $O_i = \frac{1}{m_i} \sum_{j=0}^{m_i} R_{i,j}$ is the observed average response (R) of the neuron over m presentations of the Gabor stimulus at location i, and $E_i = \frac{\sum_i^n \sum_j^{m_i} R_{i,j}}{\sum_i^n m_i}$ is the expected (grand average) response per stimulus presentation. A *p*-value was then calculated for each cell by comparing the test statistic against a null distribution of 1,000 test statistics, each computed from the cell's responses after shuffling the locations across all presentations.

Receptive field azimuth, elevation, and area: calculated from the smoothed, thresholded version of the receptive field.

DATA PROCESSING PIPELINE

Data for each session was uploaded to the Allen Institute Laboratory Information Management System (LIMS). Each dataset was run through the same series of processing steps using a set of project-specific workflows for temporal alignment, LFP downsampling, and generating NWB files and stimulus metrics. Out of 61 sessions entering the processing pipeline, 58 resulted in successful NWB file generation. The 3 processing failures were due to mismatches in session identifiers or expected file structures that prevented the workflow from completing.

NWB FILE CONTENTS

Data is shared in Neurodata Without Borders format, a standardized format for neurophysiology data{Teeters 2015}.

NWB files contain the following information

- Spike times, amplitudes, and mean waveforms for all units
- Waveform and quality metrics for all units
- Running velocity, pupil diameter, and direction of gaze information
- Stimulus presentation table with timing and parameters for each stimulus
- Table with timing of the optogenetic stimulus
- Times of any invalid intervals in the dataset
- LFP for all probes
- Current source density plot for the flash stimulus, calculated from the LFP data prior to downsampling
- Session metadata including time of acquisition, mouse strain, and rig ID

Each session has one file for all spike data, behavior data, metadata, and stimulus information (ranging in size from 1.7 GB to 3.2 GB, mean of 2.5 GB). LFP and current source density data are distributed across separate files for each probe (min = 0.9 GB, max = 2.7 GB, mean = 2.2 GB).

CODE AVAILABILITY

Code for data acquisition, processing, and analysis is available in the following repositories:

Purpose	GitHub Repository
Data pre-processing and unit metrics	AllenInstitute/ecephys_spike_sorting
Spike sorting	Mouseland/Kilosort2
OPT data acquisition and registration	AllenInstitute/AIBSOPT
Stimulus metrics and data packaging	AllenInstitute/AllenSDK
Neuropixels data acquisition	open-ephys/plugin-GUI open-ephys/neuropixels-3a open-ephys/neuropixels-PXI

OPEN-SOURCE SOFTWARE LIBRARIES

NumPy (van der Walt et al., 2011)
SciPy (Jones et al., 2001)
IPython (Pérez and Granger, 2007)
Matplotlib (Hunter, 2007)
Pandas (McKinney, 2010)
xarray (Hoyer and Hamman, 2017)
scikit-learn (Pedregosa et al., 2012)
VTK (Schroeder et al., 2006)
DeepLabCut (Mathis et al., 2018; Nath et al., 2019)
tifffile - https://pypi.org/project/tifffile/
cmocean - https://matplotlib.org/cmocean/
Jupyter - https://jupyter.org/
pynwb - https://pynwb.readthedocs.io/en/stable/

REFERENCES

Chung, J.E., Magland, J.F., Barnett, A.H., Tolosa, V.M., Tooker, A.C., Lee, K.Y., Shah, K.G., Felix, S.H., Frank, L.M., and Greengard, L.F. (2017). A fully automated approach to spike sorting. Neuron *95*, 1381-1394.e6.

Edelstein, A.D., Tsuchida, M.A., Amodaj, N., Pinkard, H., Vale, R.D., and Stuurman, N. (2014). Advanced methods of microscope control using μManager software. J Biol Methods *1*, 10.

Fiáth, R., Márton, A.L., Mátyás, F., Pinke, D., Márton, G., Tóth, K., and Ulbert, I. (2019). Slow insertion of silicon probes improves the quality of acute neuronal recordings. Sci Rep *9*, 111.

Garrett, M.E., Nauhaus, I., Marshel, J.H., and Callaway, E.M. (2014). Topography and areal organization of mouse visual cortex. Journal of Neuroscience *34*, 12587–12600.

Goldey, G.J., Roumis, D.K., Glickfeld, L.L., Kerlin, A.M., Reid, R.C., Bonin, V., Schafer, D.P., and Andermann, M.L. (2014). Removable cranial windows for long-term imaging in awake mice. Nat Protoc *9*, 2515–2538.

van Hateren, J.H., and van der Schaaf, A. (1998). Independent component filters of natural images compared with simple cells in primary visual cortex. Proceedings of the Royal Society of London. Series B: Biological Sciences *7*, 359–366.

Hill, D.N., Mehta, S.B., and Kleinfeld, D. (2011). Quality metrics to accompany spike sorting of extracellular signals. Journal of Neuroscience *31*, 8699–8705.

Hoyer, S., and Hamman, J. (2017). xarray: N-D labeled arrays and datasets in Python. Journal of Open Research Software *5*, 10.

Hunter, J.D. (2007). Matplotlib: a 2D graphics environment. Computing in Science & Engineering *9*, 90–95.

Jones, E., Oliphant, E., Peterson, P, and et al. (2001). SciPy: open source scientific tools for Python.

Juavinett, A.L., Nauhaus, I., Garrett, M.E., Zhuang, J., and Callaway, E.M. (2017). Automated identification of mouse visual areas with intrinsic signal imaging. Nat Protoc *12*, 32–43.

Jun, J.J., Steinmetz, N.A., Siegle, J.H., Denman, D.J., Bauza, M., Barbarits, B., Lee, A.K., Anastassiou, C.A., Andrei, A., Aydın, Ç., et al. (2017). Fully integrated silicon probes for high-density recording of neural activity. Nature *551*, 232–236.

Kalatsky, V.A., and Stryker, M.P. (2003). New paradigm for optical imaging: temporally encoded maps of intrinsic signal. Neuron *38*, 529–545.

Madisen, L., Mao, T., Koch, H., Zhuo, J., Berenyi, A., Fujisawa, S., Hsu, Y.-W.A., Garcia, A.J., Gu, X., Zanella, S., et al. (2012). A toolbox of Cre-dependent optogenetic transgenic mice for light-induced activation and silencing. Nature Neuroscience *15*, 793–802.

Marshel, J.H., Garrett, M.E., Nauhaus, I., and Callaway, E.M. (2011). Functional specialization of seven mouse visual cortical areas. Neuron *72*, 1040–1054.

Martin, D., Fowlkes, C., Tal, D., and Malik, J. (2001). A database of human segmented natural images and its application to evaluating segmentation algorithms and measuring ecological statistics. In Proceedings of the Eighth IEEE International Conference on Computational Vision, pp. 416–423.

Mathis, A., Mamidanna, P., Cury, K.M., Abe, T., Murthy, V.N., Mathis, M.W., and Bethge, M. (2018). DeepLabCut: markerless pose estimation of user-defined body parts with deep learning. Nature Neuroscience *21*, 1281–1289.

Matteucci, G., Bellacosa Marotti, R., Riggi, M., Rosselli, F.B., and Zoccolan, D. (2019). Nonlinear processing of shape information in rat lateral extrastriate cortex. J. Neurosci. 1938–18.

McKinney, W. (2010). Data structures for statistical computing in Python. In Proceedings of the 9th Python in Science Conference, pp. 51–56.

Nath, T., Mathis, A., Chen, A.C., Patel, A., Bethge, M., and Mathis, M.W. (2019). Using DeepLabCut for 3D markerless pose estimation across species and behaviors. Nat Protoc *14*, 2152–2176.

Newman, J.P., Fong, M., Millard, D.C., Whitmire, C.J., Stanley, G.B., and Potter, S.M. (2015). Optogenetic feedback control of neural activity. *4*, e07192.

Nguyen, D., Marchand, P.J., Planchette, A.L., Nilsson, J., Sison, M., Extermann, J., Lopez, A., Sylwestrzak, M., Sordet-Dessimoz, J., Schmidt-Christensen, A., et al. (2017). Optical projection tomography for rapid whole mouse brain imaging. Biomed. Opt. Express *8*, 5637.

Olmos, A., and Kingdom, F.A.A. (2004). A biologically inspired algorithm for the recovery of shading and reflectance images. Perception *33*, 1463–1473.

Oommen, B., and Stahl, J.S. (2008). Eye orientation during static tilts and its relationship to spontaneous head pitch in the laboratory mouse. Brain Research *1193*, 57–66.

Pachitariu, M., Steinmetz, N., Kadir, S., Carandini, M., and Harris, K.D. (2016). Kilosort: realtime spike-sorting for extracellular electrophysiology with hundreds of channels. BioRxiv.

Pedregosa, F., Varoquaux, G., Gramfort, A., Michel, V., Thirion, B., Grisel, O., Blondel, M., Müller, A., Nothman, J., Louppe, G., et al. (2012). Scikit-learn: machine learning in python. ArXiv.

Peirce, J.W. (2007). PsychoPy—Psychophysics software in Python. Journal of Neuroscience Methods 6.

Pérez, F., and Granger, B.E. (2007). IPython: a system for interactive scientific computing. Computing in Science & Engineering *9*, 21–29.

Quian Quiroga, R., Reddy, L., Koch, C., and Fried, I. (2007). Decoding visual inputs from multiple neurons in the human temporal lobe. Journal of Neurophysiology *98*, 1997–2007.

Renier, N., Wu, Z., Simon, D.J., Yang, J., Ariel, P., and Tessier-Lavigne, M. (2014). iDISCO: A Simple, Rapid Method to Immunolabel Large Tissue Samples for Volume Imaging. Cell *159*, 896–910.

Schmitzer-Torbert, N., Jackson, J., Henze, D., Harris, K., and Redish, A.D. (2005). Quantitative measures of cluster quality for use in extracellular recordings. Neuroscience *131*, 1–11.

Schroeder, W., Martin, K., and Lorensen, B. (2006). The Visualization Toolkit.

Sharpe, J. (2002). Optical Projection Tomography as a Tool for 3D Microscopy and Gene Expression Studies. Science *296*, 541–545.

Siegle, J.H., López, A.C., Patel, Y.A., Abramov, K., Ohayon, S., and Voigts, J. (2017). Open Ephys: an open-source, plugin-based platform for multichannel electrophysiology. Journal of Neural Engineering *14*, 045003.

Stringer, C., Pachitariu, M., Steinmetz, N., Reddy, C.B., Carandini, M., and Harris, K.D. (2019). Spontaneous behaviors drive multidimensional, brainwide activity. Science *364*, eaav7893.

Teeters, J.L., Godfrey, K., Young, R., Dang, C., Friedsam, C., Wark, B., Asari, H., Peron, S., Li, N., Peyrache, A., et al. (2015). Neurodata Without Borders: creating a common data format for neurophysiology. Neuron *88*, 629–634.

de Vries, S.E.J., Lecoq, J., Buice, M.A., Groblewski, P.A., Ocker, G.K., Oliver, M., Feng, D., Cain, N., Ledochowitsch, P., Millman, D., et al. (2018). A large-scale, standardized physiological survey reveals higher order coding throughout the mouse visual cortex. BioRxiv.

van der Walt, S., Colbert, S.C., and Varoquaux, G. (2011). The NumPy array: a structure for efficient numerical computation. Computing in Science & Engineering *13*, 22–30.

Welles, O. (1958). Touch of Evil (Universal - International).

Wong, M.D., Dazai, J., Walls, J.R., Gale, N.W., and Henkelman, R.M. (2013). Design and Implementation of a Custom Built Optical Projection Tomography System. PLoS ONE *8*, e73491.

Wypych, M., Wang, C., Nagy, A., Benedek, G., Dreher, B., and Waleszczyk, W.J. (2012). Standardized F1 – A consistent measure of strength of modulation of visual responses to sine-wave drifting gratings. Vision Research *72*, 14–33.

Zhang, F., Wang, L.-P., Boyden, E.S., and Deisseroth, K. (2006). Channelrhodopsin-2 and optical control of excitable cells. Nat Methods *3*, 785–792.